extremely low solubilities of sulphides in water. Sullivan (1957) gave partial support for Brown's idea, but felt that the heat of formation and E.M.F. series decided which metals occurred as silicates, oxides, sulphides and native metals respectively. Krauskopf (1967) thought that the transport of heavy sulphides is unlikely, but that the transport of heavy metals may take place in the volatile state. Jacobsen (1967) in discussing the ore deposits at Artonvilla states that 'mineralogical evidence suggests that the hydrothermal alteration was caused by watery solutions containing Na_2O, CaO, Al_2O_3, K_2O, CO_2 and SiO_2'. Whether these constituents were part of the primary solution or represent absorbed matter from the deeper portions of the conduit is not known. Jacobsen does not rule out the possibility that the sulphides at Artonvilla were transported in the volatilized state.

c. Composition and pH of mineralizing fluids

The composition of hydrothermal solutions as established by several authors from a study of volcanic emanations is predominantly H_2O, S, Cl, F, B, P and CO_2. The pH of hydrothermal solutions is probably seven or more, since if the solutions were acid they would cause more intense wall rock alteration in carbonate than silicate host rocks as calcite should be destroyed. Garrels (1944) concluded that while acid solutions are incapable of metal transport alkaline solutions may transport metals in a complexed state.

d. Mineralizing solutions at Roodekraal

The writer considers that initially, at great depths, the ore solutions were sulphides in the vapourized state and that as they rose they heated the surrounding and overlying rocks to such an extent that much of the water present was driven out of the rocks. The hot aqueous solutions thus formed acted as the vanguard of the ore solutions and probably contained CO_2, K_2O and Na_2O. The secondary gangue minerals were formed largely at the same time as the sulphide minerals, but over a far greater area of rock because of the higher mobility of the aqueous solutions. As crystallisation proceeded the lower temperature components were concentrated in the areas of lower pressure.

5. Source of Mineralizing Fluids

The author has concluded that the Roodekraal Igneous Complex is post-Transvaal and pre-Pilandsberg in age, and since the mineralization probably followed shortly after the consolidation of the rock type, it

must be pre-Pilandsberg in age.

Of the rock types present in the Roodekraal Igneous Complex itself there is only one which could possibly have acted as a source of mineralizing solutions, this being the coarse pyroxene diorite. Hydrothermal alteration was much less intense in the coarse pyroxene diorite than in the other rock types. The coarse pyroxene diorite was the last major rock type to be emplaced and is thought to be the parent body of the dioritic-pegmatite and dioritic-aplite veins. However, if the coarse pyroxene diorite had an excess of volatiles, it would be expected that amphibole, and not pyroxene, would be the stable mafic mineral present (Bowen, 1928).

The most likely source for the ore forming solutions however, is not logically to be found at Roodekraal, since copper sulphides and malachite stainings have been found at several other points around the Vredefort Ring Structure e.g. Bisschoff (1972b) states that copper sulphides are present in the Lindequesdrift intrusion and the alkali granite aplite of the Vredefort Ring Structure. Much evidence has been presented for the occurrence of a large basic body at depth beneath the Vredefort Ring Structure by such authors as Hall and Molengraaff (1925), Nel (1927), Truter (1941), Bisschoff (1950) and (1970) and du Toit (1966). It seems probable that sulphides were differentiated from this magma body shortly after the widespread injection of pseudotachylite had taken place.

VI. CONCLUSIONS

1. The Roodekraal Igneous Complex was formed after the deposition of the sedimentary rocks making up the Magaliesberg Stage of the Pretoria Series, and before the introduction of pseudotachylite approximately 1 970 million years ago. Thus this Complex was formed at a similar time to the emplacement of the Bushveld Igneous Complex. A large hidden magma body beneath the Vredefort Ring Structure is probably the parent of the Roodekraal Igneous Complex and all the other igneous bodies within the Ring Structure. The presence of a hidden magma body has been postulated by authors such as Hall and Molengraaff (1925), Nel (1927), Truter (1941), Bisschoff (1950) and (1970) and du Toit (1966).

2. The rock types at Roodekraal were found to have undergone virtually no folding or tilting since they were extruded and for the reasons detailed under the section entitled 'Formation of the Roodekraal Igneous Complex', the author concludes that the Roodekraal Igneous Complex was emplaced after the deformation of the sedimentary rocks of the Vredefort Ring Structure, within a tectonic basin formed by the intersection of two synclinal axes. Since no pillow structures or other evidence of extrusion under water are found at Roodekraal, the lavas are regarded as having been extruded onto a land surface.

3. As regards sub-division of the rock types present at Roodekraal the author has concluded that the major rock types may be divided into two main groups, namely the andesite/diorite group and the pyroxene andesite/diorite group. The division between these two groups was made principally on a basis of a distinctly different mineralogy, with augite present in far greater proportion within the pyroxene andesite/diorite group. However there are many other differences between these groups, such as a distinctly different geochemistry, well demonstrated by the presence of two differentiation trends on the 'Pearce diagrams' (Fig. xv (a) and (b) in Appendix II) and a markedly different field appearance, with pyroxene andesite/diorite group being generally darker in colour and always strongly porphyritic, whereas rocks of the andesite/diorite group are usually equigranular.

4. The sequence of emplacement for the rock types of the Roodekraal Igneous Complex began with the massive andesite followed by the amygdaloidal andesite, equigranular diorite, pyroxene andesite, fine pyroxene diorite, coarse pyroxene diorite, olivine gabbro, dioritic-aplite, dioritic-pegmatite, dolerite, syenite, pseudotachylite and syenite-porphyry. This sequence is in agreement with that suggested by Bisschoff (1950) except that it has been extended by the author to include five more rock types. Four of these rock types, namely massive andesite, pyroxene andesite, olivine gabbro and dioritic-pegmatite, have not been described before while the fifth rock type is pseudotachylite. The massive andesite underlies the amygdaloidal andesite and is believed to be the first rock type to have been emplaced, while the pyroxene andesite is the extrusive equivalent of the fine pyroxene diorite. The olivine gabbro formed as a cumulate rock immediately after the emplacement of the coarse pyroxene diorite, and the dioritic-pegmatite, which forms as dilation vein fillings associated with dioritic-aplite, probably crystallised from aqueous fluids shortly after the formation of the olivine gabbro.

5. The syenite-porphyry was the last rock type to be emplaced since, it is not cut by pseudotachylite veins, it has very pronounced chill zones and no hydrothermal alteration. This rock type has a similar macroscopic appearance and chemical composition to rocks of the Pilandsberg dike swarm and is therefore regarded as being of Pilandsberg age.

6. From a study of the geochemistry of the various rock types, relying mainly on the procedures of Irvine and Baragar (1971), Chayes (1965 and 1966) and Yoder and Tilley (1962) it was decided that the parent magma from which the rock types of the Roodekraal Igneous Complex were derived was probably tholeiitic. An earlier suite of tholeiitic rocks is present within the Vredefort Ring Structure and was most likely derived from the same parent magma as the Roodekraal Igneous Complex. The presence of this earlier suite of tholeiitic rocks is in agreement with the conclusion that the Roodekraal Igneous Complex had a tholeiitic parent magma.

7. The sulphide bodies are restricted in their occurrence to a structural trap within the amygdaloidal andesite. The elements comprising this structural trap are a suitable host rock, namely the amygdaloidal andesite, a pyroxene andesite cap rock with an

impervious chill zone above the deposits, and an equigranular diorite sill and coarsely crystalline andesite below. Within these structural traps the sulphide bodies are mainly concentrated along normal faults.

8. The sulphide bodies have apparently concentric zones of hydrothermal alteration around them, the chief process of hydrothermal alteration involved was the conversion of the mafic minerals to biotite. The hydrothermal alteration around the sulphide bodies was thus restricted to the 'phyllic facies' of alteration as described by Burnham (1962), and was completely unconnected with widespread deuteric alteration which occurred through almost the entire volume of the rocks present at Roodekraal. The deuteric alteration involved such effects as the conversion of augite to uralite and andesine to albite.

9. The prominent zoning of the ore and gangue minerals present within the sulphide replacement bodies themselves is the reverse of the normal sequence as established by authors such as Emmons (1924), Blanchard (1927), Graton and Bowditch (1936), Parks (1955), Sales and Meyer (1950), Schwartz (1956) and Parks and McDiarmid (1964), but agrees very closely with the mineral zoning present at Artonvilla mine in the Messina district as described by Jacobsen (1967). The author concluded that there are two distinctly different zonal sequences, firstly, the normal zonal sequence which occurs in open space filling deposits formed at low pressure and secondly, the reversed zonal sequence which occurs at higher pressures in replacement deposits such as Artonvilla and Roodekraal.

10. Although the sulphide minerals present at Roodekraal were deposited over a wide range of temperatures, from climatic temperatures for azurite, malachite and cuprite to temperatures in excess of 400°C for pyrite and pyrrhotite, the sulphide bodies are considered to be epithermal because they were emplaced very close to the surface.

11. Copper sulphides and malachite stainings have been found at several places within the Vredefort Ring Structure, thus it seems that the sulphides were differentiated from the hidden magma body. Since sulphides replace the pseudotachylite they must have differentiated after the injection of pseudotachylite had taken place. The writer concluded that the ore solutions were sulphides in vapourized state, and that as they rose they heated the overlying rocks to such an extent that much of the water present was driven out of the rocks.

The hot aqueous solutions thus formed acted as the vanguard of the ore solutions and brought about the hydrothermal alteration associated with ore deposition.

REFERENCES

Abbott, D. and Ferguson, J. (1965) The Losberg Intrusion, Fochville, Transvaal. Trans. geol. Soc. S. Afr., 68, 31 - 52.

Allsopp, H.L. (1965) Rb - Sr and K - Ar measurements on the Great Dyke of southern Rhodesia. J. geophys. Res., 70, 977 - 984

Al'mukhamedov, A.L. (1967) Behaviour of Titanium during Differentiation of a Basaltic Magma. Geokhimiya, 1, 75 - 85.

Arhens, L.H., Pinson, W.H. and Kearns, M.M. (1952) Association of rubidium and potassium and their abundance in common igneous rocks and meteorites. Geochim. et cosmoch. Acta, 2, 229 - 242.

Arnold, R.G. and Reichen, L.E. (1962) Measurements of Metal Content of Naturally occurring, Metal-deficient Hexagonal Pyrrhotite by an X-ray Spacing Method. Amer. Miner., 47, 105 - 111.

Arnold, R.G. (1966) Mixtures of Hexagonal and Monoclinic Pyrrhotite and the Measurement of the Metal Content of Pyrrhotite by X-ray Diffraction. Amer. Miner., 51, 1221 - 1227.

Barth, T.F.W. (1952) Theoretic Petrology. John Wiley & Sons, Inc., New York, 387 p.

Bateman, A.M. (1964) Economic Mineral Deposits, Second Edition (ninth printing). John Wiley & Sons, Inc., New York, 916 p.

Bisschoff, A.A. (1950) Die Stollingsgesteente - Kompleks op Roodekraal 37, Potchefstroom Distrik. M.Sc thesis (unpublished), Potchefstroom University College for C.H.E., Potchefstroom, 65 p.

..... (1970) The petrology of the Igneous and Metamorphic Rocks in the Vredefort Dome and the adjoining parts of the Potchefstroom Syncline. D.Sc thesis (unpublished), University of Pretoria, Pretoria, 243 p.

..... (1972a) Tholeiitic Intrusions in the Vredefort Dome. Trans. geol. Soc. S. Afr., 75, 23 - 30.

..... (1972b) The Dioritic Rocks of the Vredefort Dome. Trans. geol. Soc. S. Afr., 75, 31 - 45.

Blanchard, R. (1927) Detailed Studies of Zoning in Ore Districts. Econ. Geol., 42, 543 - 545.

Bowen, N.L. (1928) The Evolution of Igneous Rocks. Princeton: Princeton Univ. Press, 332 p.

Brett, P.R. (1963) The Cu-Fe-S System. The join $Cu_{9.2}S_5$ - Cu_5FeS_4, Cu_5FeS_4 - Cu_2S, Cu_5FeS_4 - $CuFeS_{2-x}$. Annual report of the Director, Geoph. Lab., Carnegie Inst. of Washington, 193 - 196.

..... (1964) Experimental Data from the System Cu-Fe-S and their bearing on Exsolution Textures in Ores. Econ. Geol., 59, 1241 - 1269.

Brown, A.C. (1971) Zonin in the White Pine Copper District, Ontonagon County, Michigan. Econ. Geol., 66, No. 4, 543 - 573.

Brown, J.S. (1950) Ore Genesis. Thomas Murby & Co., London, 204 p.

Buddington, A.F. and Lindsay, D.H. (1964) Iron - Titanium Oxide Minerals and Synthetic Equivalents. J. Pet., Oxford, 5, 310 - 355.

Buerger, N.W (1934) The Unmixing of Chalcopyrite from Sphalerite. Amer. Miner., 19, 525 - 530.

..... (1941) The Chalcocite Problem. Econ. Geol., 36, 19 - 44.

Burke (1966 - 1967) Results of Vicker's Hardness Measurements on Ore Minerals, achieved in Different Laboratories since 1956, mentioned in "Second Summary of Vicker's Hardness Measurements" by W. Uytenbogaardt. Publication of Department of Mineralogy and Petrology, Institute of earth sciences, Free University, 1085 De Boelelaan - Amsterdam 11 Netherlands, 15 p.

Burnham, C.W. (1962) Facies and Types of Hydrothermal Alteration. Econ. Geol., 57, 768 - 784.

Caillère, S. (1935) Sur les caracèteres specifiques de la bowlingite. Compt. Rend. Acad. Sci. Paris, 200, p. 1483. quoted in Deer, Howie & Zussman (1967), 1, p. 29.

..... and Hénin, S. (1951) The Properties and Identification of Saponite (bowlingite). Clay Miner. Bull., 1, 138 - 144.

Chayes, F. (1955) Potash Feldspar as a by product of the Biotite - Chlorite Transformation. J. Geol., 63, 75 - 82.

..... (1965) Statistical Petrography. Carneg. Inst. Wash. Year Book, 64, 153 - 165.

..... (1966) Alkaline and Subalkaline Basalts. Amer. J. Sci., 264, 128 - 145.

Coleman, L.C. (1957) Mineralogy of Giant Yellow-knife gold mine, Yellow-knife, N.W.T. Econ. Geol., 52, 400 - 425.

Daly, R.A. (1933) Igneous Rocks and the Depths of the Earth. McGraw-Hill Book Company, New York, 598 p.

Danchin, R.V. and Ferguson, J. (1970) The Geochemistry of the Losberg Intrusion, Fochville, Transvaal. Geol. Soc. S Afr., Spec. Publ. 1, 689 - 714.

Davies, R.D., Allsopp, H.L., Erlank, A. J. and Manton, W.I. (1970) Sr. isotopic studies on various layered mafic intrusions in Southern Africa. Geol. Soc. S. Afr., Spec. Publ. 1, 576 - 591.

Deer, W.A., Howie, R.A. and Zussman, J. (1967) Rock - Forming Minerals, (5 volumes). Longmans, Green & Co. Ltd., London, 1788 p.

De Sitter, L.U. (1964) Structural Geology, (2nd Edition). McGraw-Hill Book Company, New York, 552 p.

Du Toit, A.L. (1966) Geology of South Africa, Third edition edited and prepared by S.H. Houghton. Oliver & Boyd, London, 611 p.

Edwards, A.B. (1965) Textures of Ore Minerals and their Significance, (Reprint with corrections) 4th Edition. Austral. Inst. Min. Met., Brown, Prior and Anderson Pty. Ltd., Australia, 242 p.

Emmons, W.H. (1924) Primary Downward Changes in Ore Deposits. Amer. Inst. Min. (Metall.) Engs., Pamphlet No. 1319 M.

Eriksson, K.A. (1971) A basin analysis of the Transvaal Sequence in the Potchefstroom synclinorium, Transvaal and Orange Free State. M.Sc. thesis (unpublished), University of the Witwatersrand, Johannesburg, 79 p.

Fenner, C.N. (1933) Pneumatolitic Processes in the Formation of Minerals and Ores. Amer. Inst. (Metall.) Engs. Lindgren Vol., 58 - 105.

Folinsbee, R.E. (1949) Determination of Reflectivity of the Ore Minerals. Econ. Geol., 44, 425 - 436.

Garrels, R.M. (1944) Solubility of Metal Sulphides in Dilute Vein-formi Solutions. Econ. Geol., 39, 472 - 483.

Graton, L.C. and Bowditch, S.I. (1936) Alkali and Acid Solutions in Hypogene Zoning at Cerro de Pasco. Econ. Geol., 31, 651 - 698.

Graton, L.C. (1933) The Hydrothermal Depth Zones. Amer. Inst. Min. (Metall.) Engs. Lindgren Vol., 181 - 197.

..... (1940) Nature of the Ore Forming Fluids. Econ. Geol., 35; 197 - 358.

Grout, F.F. (1932) Petrography and Petrology. McGraw-Hill Book Company, New York, 300 p.

Hall, A.L. and Molengraff, G.A.F. (1925) The Vredefort mountain land in the southern Transvaal and northern Orange Free State. Shaler Memorial Series, Koninkl. Akad. Wetensch. Amsterdam, Verh. 24, 183 p.

Hargraves, R.B. (1970) Paleomagnetic Evidence Relevant to the origin of the Vredefort Ring. J. Geol., 78, 253 - 264.

Heinrich, W. Wm. (1965) Composite Aplite - pegmatites of the Franklin Sylvia District of North Carolina. Amer. Miner., 50, 1681 - 1697.

Helgeson, H.C. (1964) Complexing and Hydrothermal ore Deposition. Permagon Press, Oxford, 128 p.

Hess, H.H. (1933) Serpentinization : origin of certain chrysotile asbestos, talc and soapstone deposits. Econ. Geol., 28, 634 - 658.

Holmes, A. (1920) The Nomenclature of Petrology. Murby, London, 284 p.

Irvine, T.N. and Baragar, W.R.A. (1971) A guide to the Chemical Classification of Common Volcanic Rocks. Canadian Journal of Earth Sciences, 8, number 5, 523 - 545.

Jacobsen, J.B.E. (1967) The Geology of the Artonvilla Mine, Messina District. PhD. thesis (unpublished), University of Witwatersrand, Johannesburg, 123 p.

Jahns, R.L. and Burnham, C.W. (1969) (Experimental Studies of pegmatite genesis: 1. A model for the derivation and cry[illegible]lisation of Granitic pegmatite[illegible]on. Geol., 64, 843 - 864.

Jahns, R.H. and Tuttle, O.F. (1963) Layered pegmatite - aplite intrusives. Miner. Soc. Amer., Special Paper 1, 78 - 92.

Jambor, J.L. and Smith, C.H. (1964) Olivine composition determination with small-diameter X-ray powder cameras. Miner. mag., 33, 730 - 748.

Johannsen, A. (1937) A descriptive Petrography of the Igneous Rocks, III. University of Chicago Press, Chicago, 360 p.

Kennedy, W.Q. (1933) Trends of Differentiation in Basaltic Magmas. Amer. J. Sci., 25, 239 - 256.

King, L.C. (1963) South African Scenery, (Third edition - revised). Oliver & Boyd, Edinburg and London, 340 p.

Krauskopf, K.B. (1967) Introduction to Geochemistry. McGraw-Hill Book Company, New York, 721 p.

Kullerud, G., Busseck, P.R., Doe, B.R. and Troften, P.F. (1963) Heating experiments on monoclinic pyrrhotites. Annual Report of Director Geoph. Lab., Carnegie Inst. of Washington, 210 - 213.

Kuno, H. (1968) Differentiation of basaltic magmas. Basalts (The Poldervaart treatise on rocks of basaltic composition), 2, 623 - 688.

Lindgren, W. (1933) Mineral Deposits, Fourth Ed. McGraw-Hill Book Company, New York, 930 p.

McElhinny, M.W., Briden, J.C., Jones, D.L. and Brock, A. (1968) Geological and geophysical implications of paleomagnetic results from Africa. Rev. Geophys., 6, 201 - 238.

Mellor, E.T. (1907) The Geology of the Central Portion of the Potchefstroom District. Ann. Rep. Geol. Surv. Tvl. for 1907., 11 - 30.

Moh, G. (1963) Low Temperature Sulphide Synthesis. Annual report of the Director, Geoph. Lab., Carnegie Inst. of Washington, 214 - 215.

Morse, S.A. (1968) Syenites. Annual Report of the Director, Geoph. Lab., Carnegie Inst. of Washington, 112 - 120.

Nel, L.T. (1927) The Geology of the country around Vredefort. Explan. Geol. map, Geol. Suv. S. Africa, Dept. Min. and Industr., Govt. Printer, Pretoria, 134 p.

Nel, L.T., Truter, F.C., Willemse, J. and Mellor, E.T. (1939) The Geology of the country around Potchefstroom and Klerksdorp. - An explanation of Sheet No. 61 (Potchefstroom), Govt., Surv., Pretoria, 156 p.

Nicolaysen, L.O., Burger, A.J. and van Niekerk, C.B. (1963) Origin of the Vredefort Ring Structure in the light of new isotopic data. Int. union of geod. and geoph. Program Abstract Aug. 1963.

Nockolds, S.R. and Allen, R. (1953) The Geochemistry of some Igneous Rock Series. Geochim. et cosmoch. Acta, 4, Part 1, 105 - 142.

Nockolds, S.R. (1954) Average chemical compositions of some Igneous Rocks. Bull. geol. Soc. Amer., 65, 1007 - 1032.

Ovchinnikov, L. (1963) On the participation of gases in post-magmatic ore deposition and the distinguishing of a pneumatolytic phase. Problems of Post-magmatic ore deposition, Prague, Czech. Acad. Sci. rada G.

Parks, C.F. (Jnr.) (1955) Zonal theory of Ore deposits. Econ. Geol., 50th Anniv. Vol., 226 - 248.

..... and McDiarmid, R.A. (1964) Ore deposits. W.H. Freeman and Company, San Francisco, 475 p.

Pearce, T.H. (1968) A contribution to the theory of variation diagrams. Contr. Mineral. and Petrol., 19, 142 - 157.

..... (1970) Chemical variations in the Palisade sill. J. Pet., Oxford, 11, Part 1, 15 - 32.

Philpotts, A.R. (1964) Origin of pseudotachylites. Amer. J. Sci., 262, 1008 - 1035.

Philpotts, J.A. and Schmetzler, C.C. (1969) Phenocryst-matrix partition coefficients for K, Rb, Sr and Ba, with applications to amorthosite and basalt genesis. Geochim. et cosmoch. Acta, 34, 307 - 322.

Ramdohr, P. (1955) Die Erzmineralien und Ihre verwachsungen. Akademie - Verlag - Berlin, 1174 p.

Reynolds, D.L. (1954) Fluidization as a geological process and its bearing on the problem of intrusive granites. Amer. J. Sci., 252, 577 - 614.

Sales, R.H. and Meyer, C. (1950) Interpretation of Wall-Rock alteration at Butte Montana. Colorado School of Mines. Quart., 45, No. 1 B., 261 - 273.

Schneiderhöhn, H. (1941) Lehrbuch der Erzlagerstätten-kunde. 1, Jena, 858 p.

Schwartz, G.M. (1928) Experiments bearing on bornite - chalcocite intergrowths. Econ. Geol., 23, 381 - 397,

..... (1939) The significance of bornite - chalcocite micro-textures. Econ. Geol., 34, 399 - 418.

..... (1956) Argillic alteration and ore deposits. Econ. Geol., 51, 407 - 414.

Shand, S.J. (1916) The pseudotachylyte at Parys (Orange Free State) and its relation to the "trap-sholten gneiss" and flinty crush-rock. Quart. J. geol. Soc. Lond., 72, 198 - 221.

Shand, S.J. (1950) Eruptive Rocks. Thomas Murby & Co., London, 488 p.

Short, M.N. (1940) Microscopic Determination of the Ore minerals. U.S. Geol. Surv. Bull. 914, 314 p.

Smith, F.G. (1948) The ore deposition, temperature and pressure at the McIntyre Mine Ontario. Econ. Geol., 43 627 - 636.

..... (1954) The composition of vein-forming fluids from inclusion data. Econ. Geol., 49, 205 - 210.

Smith J.V. (1956) The powder patterns and lattice parameters of plagioclase feldspars. 1. The soda-rich plagioclases. Miner. Mag., 31, 47 - 68.

Spurr, J.E. (1922) The Ore Magmas. McGraw-Hill Book Company, New York, 915 p.

Streckeisen, A.L. (1967) Classification and Nomenclature of Igneous Rock, (Final report of an inquiry). E. Schweizerbartsche Verslagsbuchhandlung, Stuttgart, 27 p.

Sullivan, C.J. (1957) Heat and temperature in ore deposition. Econ. Geol., 52 5 - 24.

Tilley, C.E. (1950) Some aspects of magmatic evolution. Quart. J. geol. Soc. Lond., 106, 37 - 61.

Truter, F.C. (1936) Observations on the geology and tectonics of a portion of the Potchefstroom district. Trans. geol. Soc. S. Afr., 39, 441 - 456.

Turner, F.J. and Verhoogen, J. (1960) Igneous and Metamorphic Petrology. McGraw-Hill Book Company, New York, 694 p.

Whitmore, D.R.E., Berry, L.G. and Hawley, J.E. (1946) Chrome Micas. Amer. Miner., 31, 1 - 21.

Wilkinson, J.F.G. (1968) The petrography of basaltic rocks. Basalts (The Poldervaart treatise on rocks of basaltic composition), 1, 163 - 214.

Wilshire, H.G. (1958) Alteration of olivine and orthopyroxenes in basic lavas and shallow intrusions. Amer. Miner., 43, 120 - 147.

Wright, T.L. (1968) II An X-ray method for determining the composition and structural state from measurement of 2 values for three reflections. Amer. Miner., 53, 88 - 96.

Yoder, H.S. and Samaha, Th.G. (1957) Olivine X-ray determinative curve. Amer. Miner., 42, 475 p.

Yoder, H.S. and Tilley, C.E. (1962) Origin of basalt magmas : An experimental study of natural and synthetic rock systems. J. Pet., Oxford, 3, 343 - 532.

Ziv, E.F. (1956) Rutilization of ilmenite under supergene conditions. Izvest. Akad. Nauk. SSSR, sér. geol., 12, 57 p., quoted in Deer, Howie and Zussman (1967), 5, 39 p.

APPENDIX I

Chemical Analyses quoted in weight per cent and C.I.P.W. Norms

Mark of Sample		RC 1	RC 2	RC 3	RC 4
ROCK TYPE		Massive Andesite	Amygdaloidal Andesite	Amygdaloidal Andesite	Amygdaloidal Andesite
	% Oxide				
Silicon	SiO_2	51,49	50,55	52,34	50,87
Aluminium	Al_2O_3	12,91	11,66	12,33	11,23
Iron (ferric)	Fe_2O_3	1,27	5,16	3,32	4,45
(ferrous)	FeO	8,64	10,49	10,38	10,36
Magnesium	MgO	3,48	2,89	2,19	3,26
Calcium	CaO	10,43	4,22	4,18	5,06
Sodium	Na_2O	6,25	4,42	5,87	4,30
Potassium	K_2O	0,44	2,69	1,48	2,19
Water (hygroscopic)	H_2O-	0,25	0,12	0,08	0,14
(combined)	H_2O+	0,83	1,20	1,18	1,55
Carbon dioxide	CO_2	0,71	3,33	3,98	3,57
Titanium	TiO_2	1,97	1,87	1,63	1,94
Phosphorus	P_2O_5	0,78	0,46	0,47	0,45
Manganese	MnO	0,19	0,19	0,24	0,21
Strontium	SrO ppm	890	470	387	431
Rubidium	Rb_2O ppm	36	67	53	65
TOTALS		99,73	99,30	99,71	99,63
NORMATIVE MINERAL	%				
Quartz			0,08		1,25
Orthoclase		2,65	17,20	9,35	14,05
Albite		39,35	42,95	56,40	41,85
Anorthite		5,98	4,38	3,13	5,30
Nepheline		10,62			
Wollastonite			6,00		7,52
Enstatite			8,64	2,39	9,76
Ferrosilite			10,90	4,55	11,10
Diopside		33,12		12,64	
Forsterite		1,15		1,43	
Fayalite		1,19		2,71	
Magnetite		1,35	5,83	3,72	5,04
Ilmenite		2,78	2,82	2,44	2,94
Apatite		1,66	1,04	1,04	1,01
Manganese ore		0,15	0,16	0,20	0,18
TOTALS		100,00	100,00	100,00	100,00

ppm = parts per million

Mark of Sample		RC 5	RC 6	RC 7	RC 8
ROCK TYPE		Amygdaloidal Andesite	Amygdaloidal Andesite	Amygdaloidal Andesite	Amygdaloidal Andesite
	% Oxide				
Silicon	SiO_2	51,53	50,96	50,98	52,25
Aluminium	Al_2O_3	11,46	11,48	11,59	11,43
Iron (ferric)	Fe_2O_3	3,55	2,62	3,88	3,09
(ferrous)	FeO	11,64	12,18	10,80	8,94
Magnesium	MgO	2,98	2,97	2,24	2,77
Calcium	CaO	4,36	4,44	4,93	5,55
Sodium	Na_2O	4,63	4,35	4,96	4,11
Potassium	K_2O	2,28	2,08	1,63	2,84
Water (hygroscopic)	H_2O-	0,14	0,15	0,32	0,16
(combined)	H_2O+	1,43	1,49	0,73	1,33
Carbon dioxide	CO_2	2,94	4,34	4,62	4,83
Titanium	TiO_2	1,94	1,92	1,80	1,76
Phosphorus	P_2O_5	0,48	0,45	0,53	0,41
Manganese	MnO	0,19	0,15	0,16	0,19
Strontium	SrO ppm	332	335	295	467
Rubidium	Rb_2O ppm	88	79	89	89
TOTALS		99,59	99,62	99,21	99,71
NORMATIVE MINERAL %					
Quartz			0,19		2,06
Orthoclase		14,50	13,40	10,50	18,30
Albite		44,65	42,65	48,65	40,25
Anorthite		4,05	6,20	4,98	4,73
Nepheline					0,45
Wollastonite			5,84		8,96
Enstatite		5,86	8,96	3,28	8,34
Ferrosilite		9,18	15,68	8,12	10,06
Diopside		12,68		14,36	
Forsterite		0,38		1,05	
Fayalite		0,58		2,61	
Magnetite		3,99	2,99	2,37	3,53
Ilmenite		2,90	2,92	2,74	2,68
Apatite		1,07	1,04	1,20	0,93
Manganese ore		0,16	0,13	0,14	0,16
TOTALS		100,00	100,00	100,00	100,00

ppm = parts per million

Mark of Sample		RC 9	RC 10	RC 11	RC 12
ROCK TYPE		Amygdaloidal Andesite	Amygdaloidal Andesite	Amygdaloidal Andesite	Amygdaloidal Andesite
% Oxide					
Silicon	SiO_2	51,73	50,20	52,08	50,52
Aluminium	Al_2O_3	11,50	11,44	12,19	11,08
Iron (ferric)	Fe_2O_3	3,89	1,44	1,50	1,51
(ferrous)	FeO	11,57	10,67	10,69	13,51
Magnesium	MgO	5,17	2,24	2,75	2,99
Calcium	CaO	4,63	7,81	4,99	4,37
Sodium	Na_2O	4,98	4,82	4,86	4,45
Potassium	K_2O	2,04	0,88	1,74	1,52
Water (hygroscopic)	H_2O-	0,26	0,43	0,12	0,23
(combined)	H_2O+	1,16	1,05	1,59	1,34
Carbon dioxide	CO_2	2,66	6,19	4,66	5,86
Titanium	TiO_2	1,74	1,60	1,64	1,74
Phosphorus	P_2O_5	0,38	0,96	0,49	0,40
Manganese	MnO	0,14	0,27	0,14	0,18
Strontium	SrO ppm	455	487	383	403
Rubidium	Rb_2O ppm	98	57	67	73
TOTALS		99,84	100,13	99,48	99,75
NORMATIVE MINERAL %					
Quartz				0,49	
Orthoclase		12,85	5,70	11,15	9,95
Albite		47,55	47,60	47,40	44,25
Anorthite		3,18	7,68	6,88	6,38
Nepheline				6,60	
Wollastonite				8,24	6,70
Enstatite		3,50	3,07	13,24	14,14
Ferrosilite		5,10	6,61		11,76
Diopside		14,88	22,36		0,41
Forsterite		2,07	0,13		0,88
Fayalite		3,00	0,29		1,76
Magnetite		4,32	1,65	2,28	2,68
Ilmenite		2,58	2,46	2,48	0,93
Apatite		0,85	2,22	1,12	0,16
Manganese ore		0,12	0,23	0,12	
TOTALS		100,00	100,00	100,00	100,00

ppm = parts per million

Mark of Sample		RC 13	RC 14	RC 15	RC 16
ROCK TYPE		Amygdaloidal Andesite	Amygdaloidal Andesite	Coarse Crystalline Andesite	Equigranular Diorite
	% Oxide				
Silicon	SiO_2	50,01	54,26	51,53	49,53
Aluminium	Al_2O_3	10,77	12,94	11,80	9,94
Iron (ferric)	Fe_2O_3	6,30	0,94	1,66	4,18
(ferrous)	FeO	12,00	12,43	10,81	12,62
Magnesium	MgO	3,32	2,04	2,44	5,69
Calcium	CaO	5,13	3,56	4,73	7,15
Sodium	Na_2O	4,48	3,95	4,99	4,40
Potassium	K_2O	1,94	1,59	1,84	1,42
Water (hygroscopic)	H_2O-	0,16	0,16	0,21	0,17
(combined)	H_2O+	0,88	1,78	1,04	1,17
Carbon dioxide	CO_2	2,12	4,45	6,31	0,53
Titanium	TiO_2	1,89	1,46	1,67	2,11
Phosphorus	P_2O_5	0,39	0,39	0,49	0,40
Manganese	MnO	0,17	0,08	0,12	0,23
Strontium	SrO ppm	320	515	344	395
Rubidium	Rb_2O ppm	73	48	83	43
TOTALS		99,60	100,09	99,68	99,68
NORMATIVE MINERAL	%				
Quartz		2,10	7,25		
Orthoclase		12,25	10,30	11,95	8,75
Albite		43,05	38,80	49,25	40,40
Anorthite		3,80	14,10	4,80	3,30
Nepheline					0,45
Wollastonite		8,04	1,00		
Enstatite		9,82	6,16	4,17	
Ferrosilite		7,70	18,14	8,17	
Diopside				14,00	24,72
Forsterite				0,66	7,31
Fayalite				1,29	6,38
Magnetite		9,40	1,08	1,91	4,56
Ilmenite		2,82	2,22	2,58	3,06
Apatite		0,88	0,88	1,12	0,88
Manganese ore		0,14	0,07	0,10	0,19
TOTALS		100,00	100,00	100,00	100,00

ppm = parts per million

Mark of Sample		RC 17	RC 18	RC 19	RC 20	RC 21
ROCK TYPE		Equi-granular Diorite	Pyroxene-Andesite	Fine Pyroxene - diorite	Fine Pyroxene - diorite	Coarse Pyroxene - diorite
	% Oxide					
Silicon	SiO_2	52,91	49,65	52,21	52,14	51,09
Aluminium	Al_2O_3	12,45	11,64	12,99	12,84	15,79
Iron (ferric)	Fe_2O_3	3,88	6,30	4,45	0,47	2,98
(ferrous)	FeO	10,37	8,46	8,96	13,22	9,29
Magnesium	MgO	3,02	4,53	3,38	4,55	2,72
Calcium	CaO	4,61	6,28	5,09	6,02	5,84
Sodium	Na_2O	5,91	4,31	5,64	4,84	5,69
Potassium	K_2O	1,76	1,79	1,49	1,72	1,19
Water (hygroscopic)	H_2O-	0,23	0,14	0,20	0,18	0,26
(combined)	H_2O+	1,27	1,24	1,48	0,24	1,56
Barium	BaO				0,09	
Carbon dioxide	CO_2	0,56	2,69	0,57		0,39
Titanium	TiO_2	1,84	1,80	1,87	1,78	1,76
Phosphorus	P_2O_5	0,46	0,47	0,56	0,63	0,74
Manganese	MnO	0,19	0,19	0,19	0,13	0,17
Strontium	SrO ppm	423	516	490	700	816
Rubidium	Rb_2O ppm	55	52	55	47	37
TOTALS		99,51	99,55	99,13	98,92	99,55
NORMATIVE MINERAL	%					
Quartz		10,75	11,80	9,15	10,40	7,25
Orthoclase		54,85	41,20	52,70	44,50	51,30
Albite		2,35	7,33	5,98	8,33	14,45
Anorthite		0,06				0,87
Nepheline						
Wollastonite			6,87	2,82	0,07	
Enstatite			3,41	2,44	0,09	
Ferrosilite		14,60	18,04	13,24	14,40	8,36
Diopside		4,10	0,32	2,53	7,34	4,44
Forsterite		5,29	0,16	2,21	10,36	5,86
Fayalite		4,20	7,01	4,85	0,51	3,21
Magnetite		2,66	2,66	2,72	2,54	2,52
Ilmenite		0,99	1,04	1,21	1,36	1,60
Apatite		0,15	0,16	0,15	0,10	0,14
Manganese ore						
TOTALS		100,00	100,00	100,00	100,00	100,00

ppm = parts per million

Mark of Sample		RC 22	RC 23	RC 24	RC 25	RC 26
ROCK TYPE		Coarse Pyroxene diorite	Dioritic-Pegmatite	Wall Rock to RC 23	Dioritic-Pegmatite	Wall Rock to RC 25
	% Oxide					
Silicon	SiO_2	48,11	58,80	50,58	51,77	40,01
Aluminium	Al_2O_3	10,35	16,09	11,25	17,24	6,02
Iron (ferric)	Fe_2O_3	16,36.	Nil	0,07	Nil	11,37
(ferrous)	FeO	1,70	5,36	12,81	9,22	9,67
Magnesium	MgO	7,70	1,60	12,90	3,15	12,50
Calcium	CaO	9,23	6,16	6,58	6,37	15,95
Sodium	Na_2O	3,12	8,59	3,10	5,80	0,79
Potassium	K_2O	0,60	0,13	0,72	0,55	0,10
Water (hygroscopic)	H_2O-	0,12	0,14	0,55	0,16	0,14
(combined)	H_2O+	Nil	2,03	0,21	0,97	0,22
Barium	BaO	0,17	0,02	0,06	0,03	0,01
Titanium	TiO_2	2,08	1,00	0,51	2,50	3,03
Phosphorus	P_2O_5	0,55	0,20	0,33	0,17	0,19
Manganese	MnO	0,21	0,05	0,13	0,08	0,18
Strontium	SrO ppm	900	700	300	800	200
Rubidium	Rb_2O ppm	13	5	27	5	5
TOTALS		100,39	100,24	99,63	98,09	100,20
NORMATIVE MINERAL %						
Quartz		4,20				
Orthoclase		3,65	0,75	4,25	3,25	0,60
Albite		28,95	65,60	27,65	52,15	3,40
Anorthite		12,93	4,90	14,58	19,43	13,10
Nepheline			6,48			2,40
Wollastonite		12,30				
Enstatite		21,98		8,59	1,92	
Ferrosilite				4,61	2,36	
Diopside			19,20	12,56	8,88	54,44
Forsterite			0,48	17,60	3,61	8,07
Fayalite			0,74	8,59	4,49	0,66
Magnetite				0,08		12,38
Ilmenite		2,72	1,38	0,70	3,50	4,40
Apatite		1,17	0,43	0,69	0,35	0,40
Manganese ore		0,17	0,04	0,10	0,06	0,15
Hematite		11,79				
Rutile		0,14				
TOTALS		100,00	100,00	100,00	100,00	100,00

ppm = parts per million

Mark of Sample		RC 27	RC 28	RC 29	RC 30	RC 31
ROCK TYPE		Dioritic-Aplite	Dolerite	Syenite	Syenite	Syenite-porphyry
	% Oxide					
Silicon	SiO_2	52,17	47,01	62,69	60,94	62,69
Aluminium	Al_2O_3	14,05	14,56	16,01	14,50	16,73
Iron (ferric)	Fe_2O_3	2,04	3,52	0,90	1,03	1,34
(ferrous)	FeO	11,75	9,76	4,47	8,27	4,29
Magnesium	MgO	3,20	5,05	0,20	0,35	0,50
Calcium	CaO	5,81	9,79	2,17	2,24	1,75
Sodium	Na_2O	5,32	2,70	6,67	5,00	6,48
Potassium	K_2O	1,18	1,88	3,42	2,71	4,22
Water (hygroscopic)	H_2O-	0,30	0,44	0,19	0,16	0,38
(combined)	H_2O+	0,16	2,43	0,61	3,60	0,12
Carbon dioxide	CO_2			1,82		
Barium	BaO	0,14	0,08		0,03	0,02
Titanium	TiO_2	2,15	2,13	0,37	0,26	0,40
Phosphorus	P_2O_5	1,00	0,23	0,11	0,06	0,14
Manganese	MnO	0,10	0,10	0,07	0,52	0,10
Strontium	SrO ppm	900	500	820	200	300
Rubi[illegible]	Rb_2O ppm	31	47	68	109	198
TOTALS		99,76	99,88	99,79	99,70	99,21
NORMATIVE MINERAL %						
Quartz				4,20	10,10	2,57
Orthoclase		7,10	11,70	20,50	16,85	24,90
Albite		48,75	25,50	60,80	47,30	58,10
Anorthite		11,23	23,15	3,70	9,63	4,10
Nepheline				2,60	0,66	1,48
Wollastonite				0,56	1,02	1,38
Enstatite		3,75	6,84	5,86	12,36	5,14
Ferrosilite		5,85	4,74			
Diopside		9,20	13,64			
Forsterite		2,60	2,87			
Fayalite		4,06	1,99			
Magnetite		2,18	3,87	0,96	1,14	1,40
Ilmenite		3,06	3,12	0,52	0,38	0,56
Apatite		2,14	2,50	0,24	0,13	0,29
Manganese ore		0,08		0,06	0,43	0,08
TOTALS		100,00	100,00	100,00	100,00	100,00

ppm = parts per million

NOTE: Analyses of RC 1 - RC 19, RC 21 and RC 29 were done by the National Institute for Metallurgy as Project K. 26/70, the remaining analyses were done by Gold Fields Laboratories (Pty) Ltd. The Sr and Rb analyses were determined to parts per ten thousand by Gold Fields Laboratories (Pty) Ltd. and parts per million by the National Institute for Metallurgy.

A P P E N D I X II

Diagrams showing the Chemical Variations present in the Rock Types of the Koodekraal Igneous Complex

Legend of Symbols used in Figures (i) to (xv)

×	Andesite
✳	Equigranular diorite
•	Pyroxene andesite/diorite
○	Other rock types

NOTE: The numbers printed next to individual rock types correspond to the RC numbers in Appendix I.

Fig. (i) AFM diagram for rocks of the Roodekraal Igneous Complex, with the dotted line dividing tholeiitic rocks from calc-alkaline rocks (modified after Irvine and Baragar 1971, p. 528).

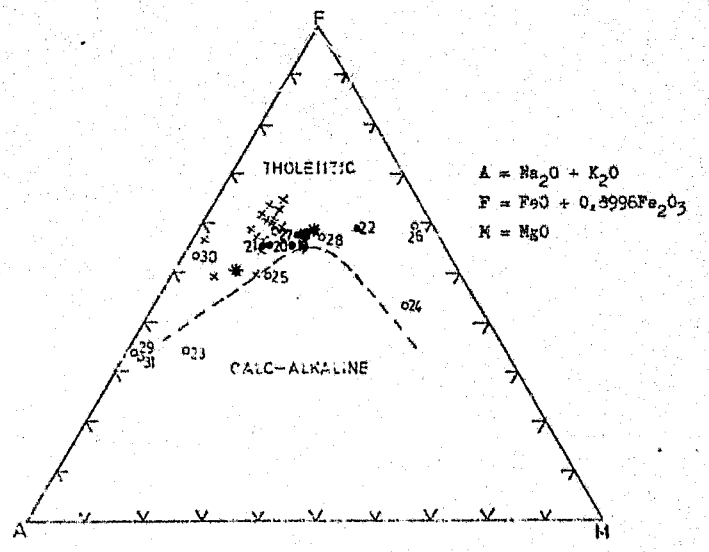

Fig. (ii) Diagram showing weight per cent Al_2O_3 plotted against normative plagioclase composition for rocks of the Roodekraal Igneous Complex, with line dividing tholeiitic rocks from calc-alkaline rocks (modified after Irvine and Baragar 1971, p. 536).

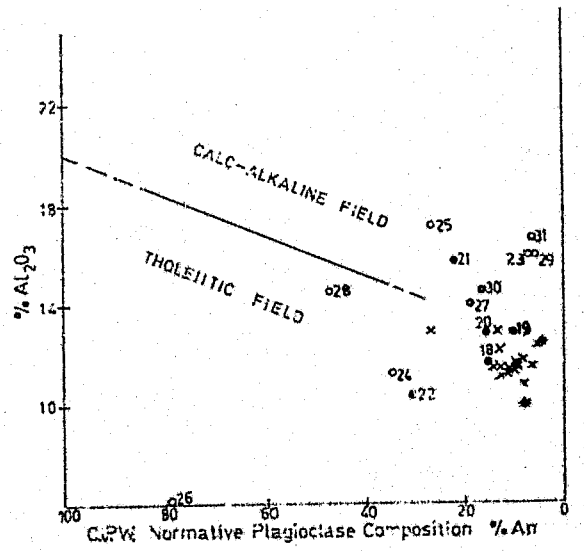

Fig. (iii) Alkalis – Silica diagram for rocks of the Roodekraal Igneous Complex, with solid line dividing the alkaline rocks from the sub-alkaline rocks (modified after Irvine and Baragar 1971, p. 532).

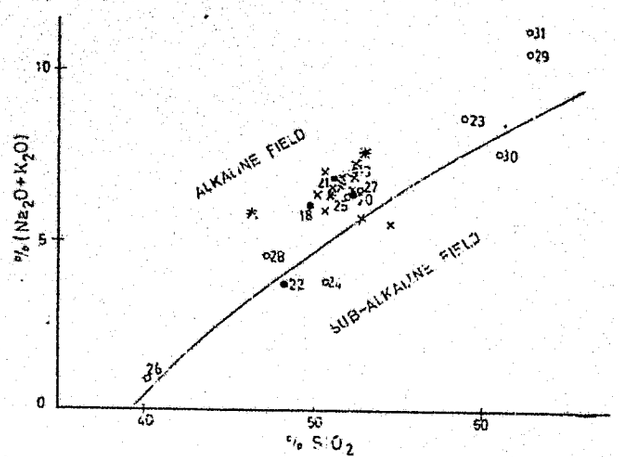

Fig. (iv) Ternary diagram of normative Cpx-Ol-Opx for rocks of the Roodekraal Igneous Complex, with straight and curved lines of Chayes (1965, 1966) dividing the alkaline rocks from the sub-alkaline rocks (modified after Irvine and Baragar 1971, p. 534).

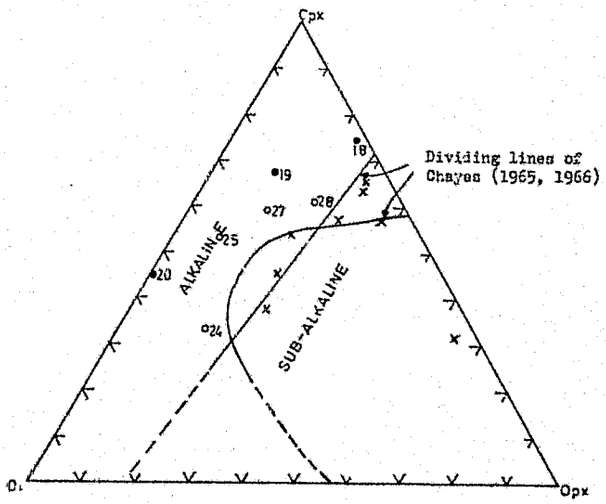

Fig. (v) Na-K-Ca ternary diagram for rocks of the Roodekraal Igneous Complex.

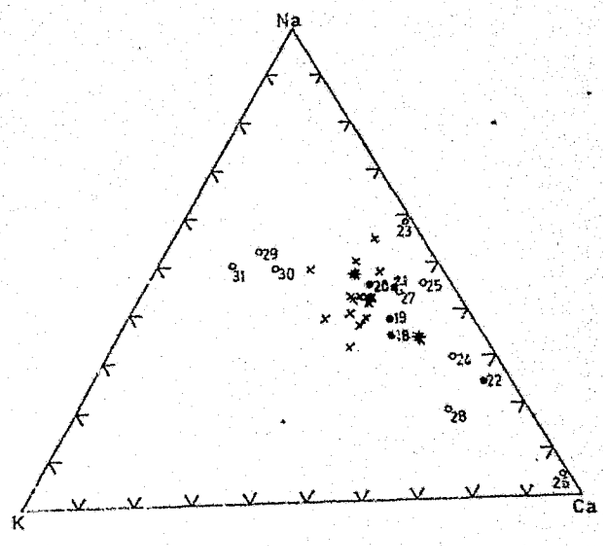

Fig. (vi) ($FeO + 0,8998Fe_2O_3$) – MgO – TiO_2 ternary diagram for rocks of the Roodekraal Igneous Complex.

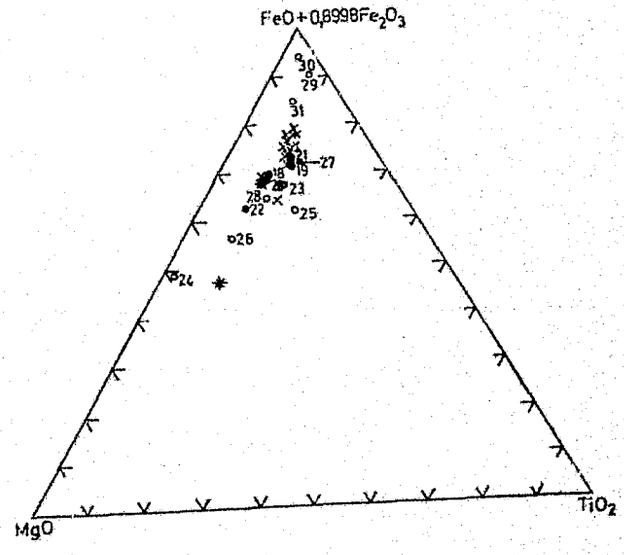

Fig. (vii) ($FeO + 0.8998Fe_2O_3 + TiO_2$) – MgO – Al_2O_3 ternary diagram for rocks of the Roodekraal Igneous Complex.

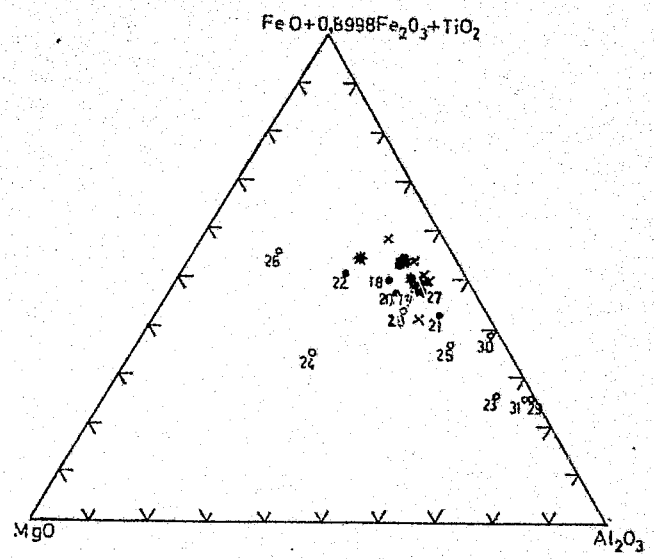

Fig. (viii) Diagram of percentage FeO plotted against Fe_2O_3 for rocks of the Roodekraal Igneous Complex.

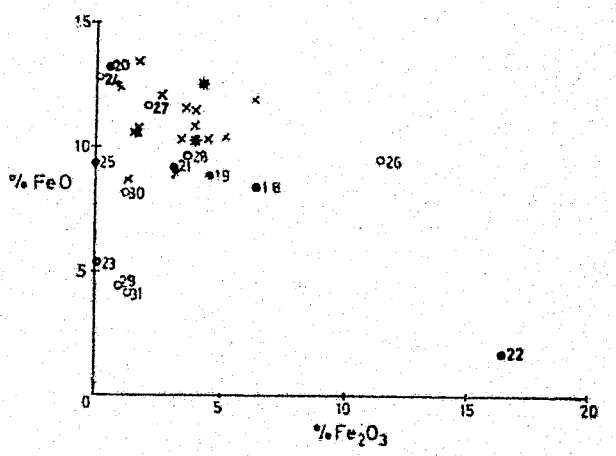

Fig. (ix) Diagram showing percentage (FeO + 0,8998Fe_2O_3) plotted against percentage TiO_2 for rocks of the Roodekraal Igneous Complex.

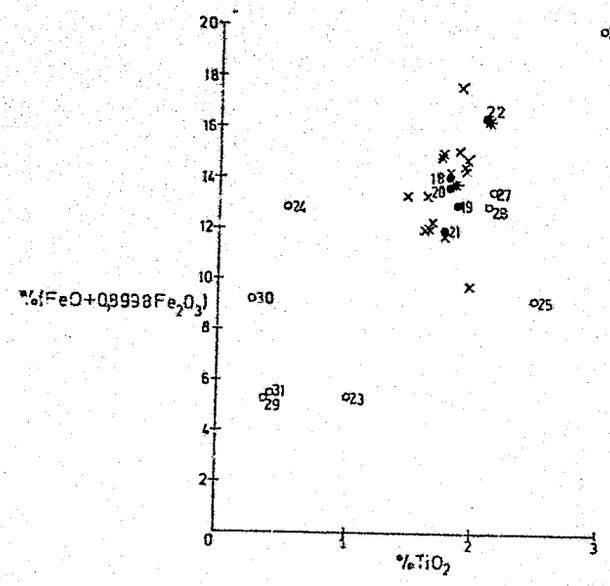

Fig. (x) Diagram of percentage MgO plotted against percentage (FeO + 0,8998Fe_2O_3) + TiO_2 for rocks of the Roodekraal Igneous Complex.

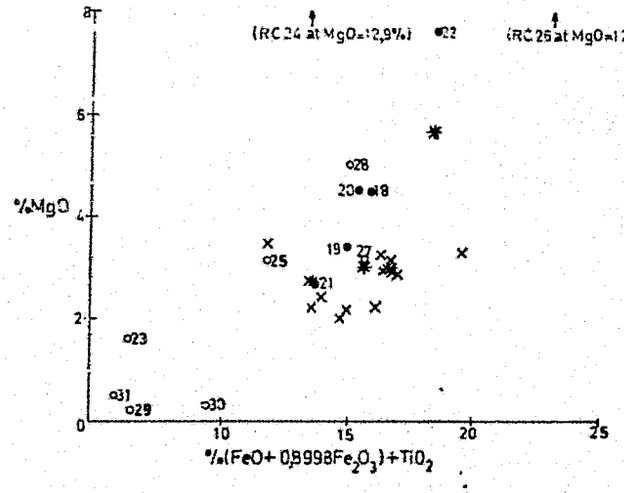

Fig. (xi) Diagram showing the relationship between the quantities of Rb and Sr present in the rocks of the Roodekraal Igneous Complex.

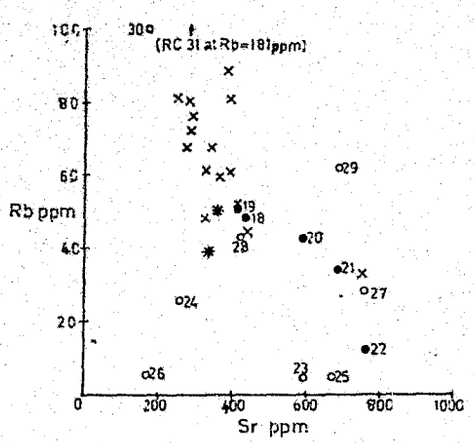

Fig. (xii) Diagram showing percentage K plotted against percentage Rb for rocks of the Roodekraal Igneous Complex. Solid line represents K/Rb = 250, which is the average value for the crustal rocks of the earth. Diagram modified after Ahrens et al. (1952, p. 240).

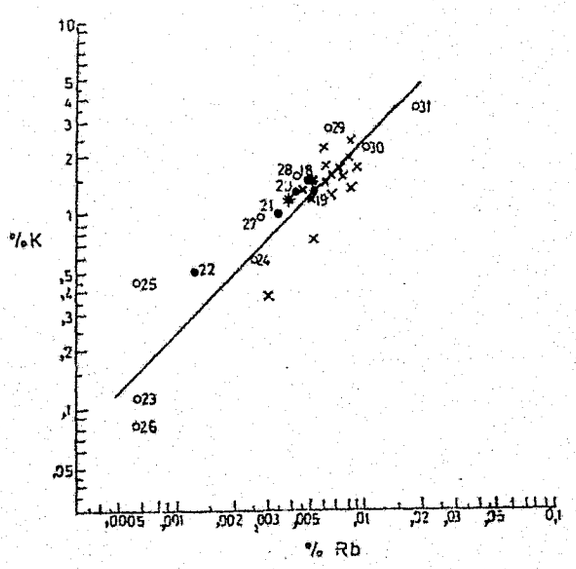

Fig. (xiii) Diagram showing percentage K plotted against Rb/Sr for rocks of the Roodekraal Igneous Complex.

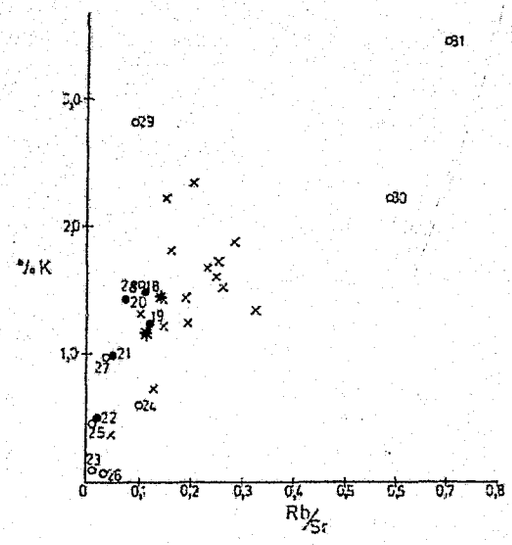

Fig. (xiv) Diagram showing percentage Cs plotted against percentage Sr for rocks of the Roodekraal Igneous Complex.

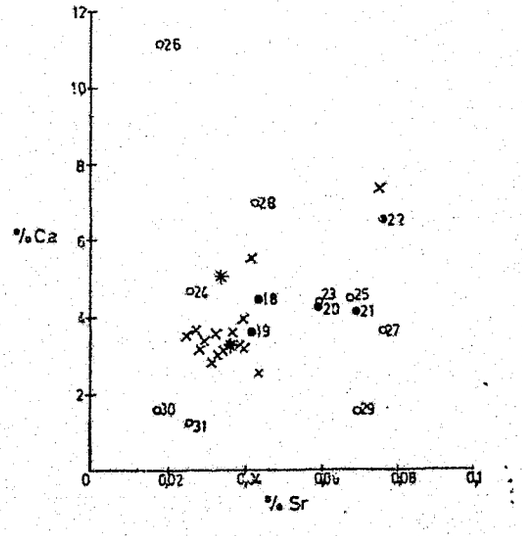

Fig. (xv) 'Pearce diagrams' of the molar ratios of MgO/Al_2O_3 plotted against SiO_2/Al_2O_3, and CaO/Al_2O_3 plotted against SiO_2/Al_2O_3 in (a) and (b) respectively. The theoretical curves for olivine and orthorhombic and monoclinic pyroxene are given next to (a) and the theoretical curves for apatite, augite and plagioclase next to (b). Both sets of theoretical curves are plotted on rectangular co-ordinates with equal divisions along both axes.

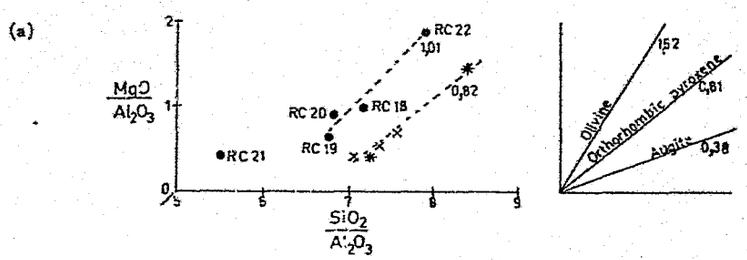

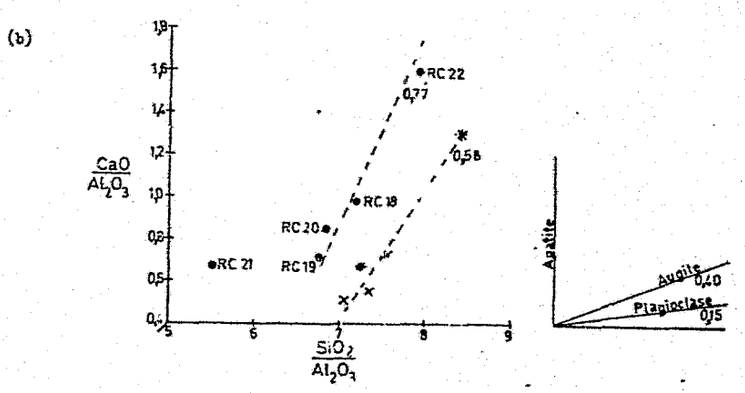

APPENDIX III

Methods Used

A. Determinative Mineralogy

In general the optical properties of the minerals were measured using the Federov Multiaxial Universal Stage and the results thus obtained were compared to the values quoted in Deer et al. (1967). The refractive indices of the minerals were determined by the liquid immersion method. A small quantity of the mineral being examined was crushed, immersed in various liquids of known refractive indices and the 'Becke line' test used to decide whether the refractive indices exhibited by a variety of mineral fragments were above or below the refractive indices of the liquids. In this way each of the refractive indices of the minerals were bracketed between two liquids, one with a higher and the other with a lower refractive index.

For X-ray analysis a small quantity of the mineral to be identified was drilled from the thin section using a diamond point. The powder thus obtained was mounted on a hair in a 57,5 millimetre diameter camera equipped with small ports and then X-rayed using copper radiation and a nickel filter. Unless otherwise stated copper radiation and a nickle filter have been used in all X-ray analyses discussed in this section. The d-values obtained from the photograph were compared with the 'Index to X-ray Powder Data File' of the American Society for Testing and Materials, Philadelphia (1965), to determine which listed mineral had d-values closest to those of the unknown mineral.

Special procedures which were used to identify specific minerals are as follows:-

1. Feldspar

To distinguish the different types of feldspar present using X-ray techniques, the method as outlined above was used and the $\bar{2}01$, 002, $\bar{1}13$, 060, $\bar{2}04$, 131 and $1\bar{3}1$ reflections obtained for the unknown feldspar were compared with the diagrams of Smith (1956, p. 65, Fig. 3) and Wright (1968, p. 91, Fig. 2). This method was used to distinguish between K-feldspar and albite, and to determine whether the plagioclase is of the high or low temperature form.

To determine the composition of the plagioclase present the extinction angle perpendicular to the a-crystallographic direction was

measured using the Federov Maxial Universal Stage and the value obtained compared with Figure 55 of Deer et al. (1967, 4, p. 138) to derive the composition of the plagioclase in percentage anorthite. To check whether the plagioclase is of the high or low temperature form the 2V and anorthite content of the plagioclase was measured and these values referred to Figure 51 of Deer et al. (1967, 4, p. 134).

2. Pyroxene

The composition of the augite was determined by referring the values obtained for β and 2V to Figure 41 of Deer et al. (1967, 2, p. 132).

3. Olivine

The composition of the olivine was determined by X-raying powder drilled from seven different olivine crystals, using iron, cobalt and copper radiation in conjunction with manganese, iron and nickel filters respectively. The values obtained for the d_{130} line were referred to the diagram of Yoder and Samaha (1957) and the values obtained for the d_{174} line to the diagram of Jambor and Smith (1964).

4. Biotite and chlorite

To determine whether smectites or other phyllosilicates with expanding lattices are associated with the biotite, a mixed sample of chlorite and biotite was prepared as a thin film on two glass slides. One glass slide was allowed to stand in the heated vapour of ethylene glycol for sixteen hours and then both of the samples were X-rayed. The reflections showed no difference in position of the peaks for the two samples, indicating that neither of the two minerals present has an expanding lattice and therefore no phyllosilicate with an expanding lattice is present.

5. Pyrrhotite

To establish the metal content of the hexagonal pyrrhotite, four grains were selected which were replacing pyrite crystals, so that sufficient sulphur would be present for the formation of a pyrrhotite with an equilibrium composition at the temperature of formation. The four grains were X-rayed and the d-values obtained were referred to the diagrams of Arnold and Reichen (1962).

6. Sphalerite

The sphalerite was X-rayed and the length of the unit cell was calculated using the d-values of thirteen reflections. The arithmetic mean was

taken of the values obtained for the thirteen reflections and gave a figure of 5,4141 A°. The value obtained was referred to the graphs of Coleman (1957) from which the content of FeS within the sphalerite was derived.

B. Geochemistry

Whenever possible the samples selected for analysis were taken from drill cores so that the rock was not weathered, channel samples were taken of narrow bodies such as pegmatite veins, dikes and sills by simply quartering the drill core. If a body was too large to channel sample, the chill zones were sampled. Wall rocks of pegmatite veins were sampled for one half of the width of the pegmatite on either side, by quartering the drill core. Samples taken from outcrop such as the samples of the syenite-porphyry, dolerite and coarse pyroxene diorite were either channel samples or samples of chill zones, depending on the width of the body sampled.

C.I.P.W. norms and the number of cations in the standard cell were calculated according to the procedures laid out in Barth (1952), the standard cell calculation being based on the number of cations associated with 160 oxygen atoms.

A P P E N D I X IV

Photographs of Structures and Textures within Drill Cores

Explanation of Plate I

Fig. 1

Photograph of amygdales which have been elongated parallel to the direction of flow.

(Magnification x 1,6)

Fig. 2

Photograph of euhedral grains of quartz (dark grey - Q) surrounded by calcite (white - Ca) within an amygdale in the andesite.

(Magnification x 4,0)

Fig. 3

Photograph of chalcedony (grey - Q) surrounding later formed calcite (white - Ca) within an amygdale.

(Magnification x 3,4)

Fig. 4

Calcite (white - Ca) surrounding later formed chlorite (dark grey - Ch) within an amygdale.

(Magnification x 9,0)

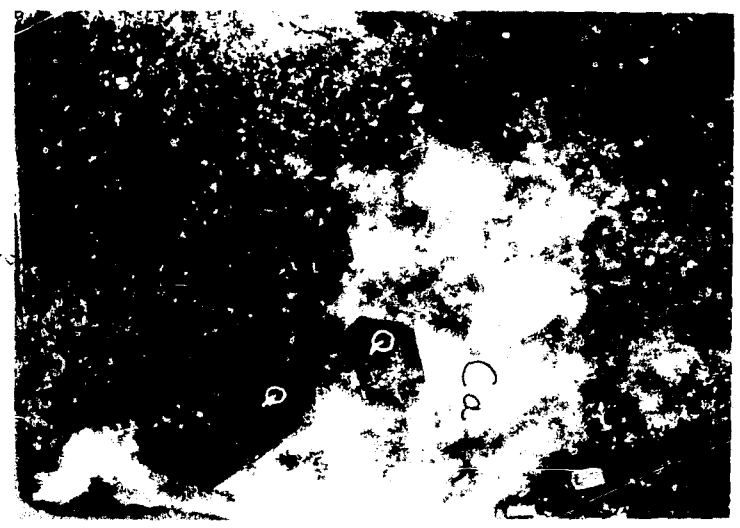

Plate I

Explanation of Plate II

Fig. 1

Photograph of feldspar crystals arranged parallel to the edge of an amygdale composed of calcite (white - Ca) and chlorite (black - Ch).

(Magnification x 5,8)

Fig. 2

Photograph showing whorl like structures of hematite and chalcedony (light grey) in andesite (black) with calcite (white).

(Magnification x 2,5)

Fig. 3

Volcanic agglomerate showing a rounded pebble of quartzite (light grey - Q) within a matrix of andesite.

(Magnification x 1,8)

Fig. 4

Volcanic breccia which has been cemented by calcite (white - Ca) and chlorite (black - Ch).

(Magnification x 2,4)

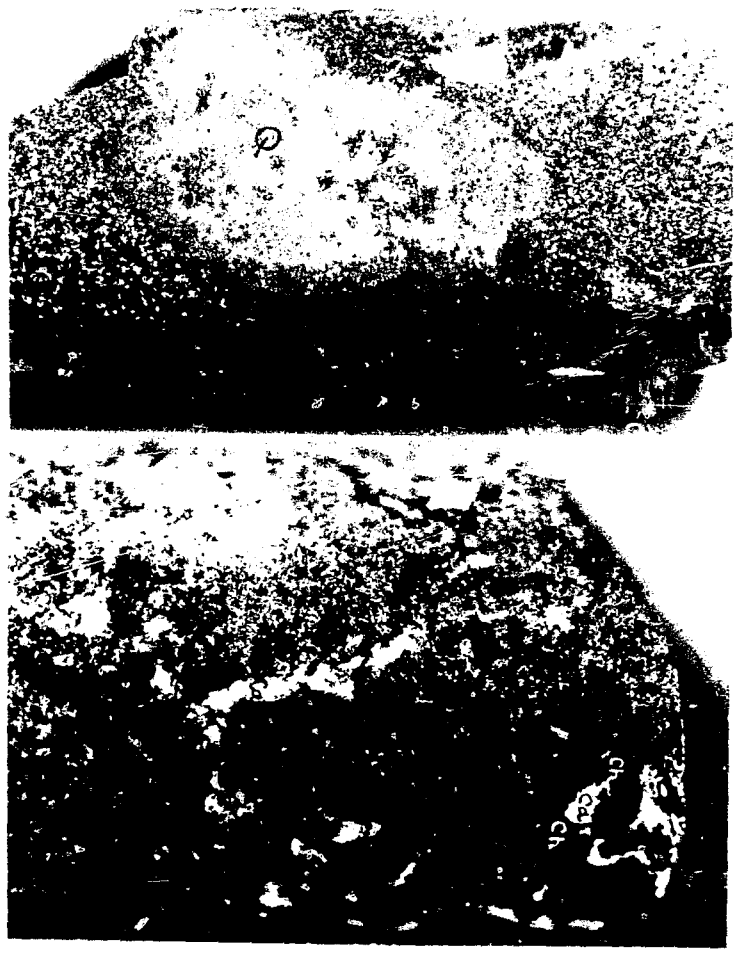
Ch
Ca
Ch
Ca
Ch
Ca

Explanation of Plate III

Fig. 1

Volcanic breccia containing fragments of coarse-grained lava (L) and calcite (white - Ca) within a matrix of fine-grained andesite.

(Magnification x 2,2)

Fig. 2

Bleached zone within the andesite which has a calcite filled vein (white - Ca) occupying its central portion.

(Magnification x 2,2)

Fig. 3

Sharp contact between dioritic-pegmatite (coarse-grained - P) and equigranular diorite wall rock (fine-grained).

(Magnification x 2,4)

Plate III

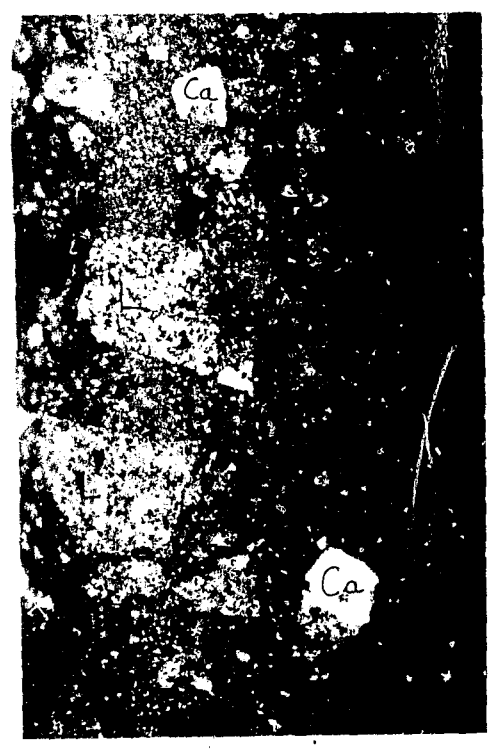

3

APPENDIX V

Photomicrographs and Photographs of Structures and Textures within Polished Sections

Explanation of Plate IV

Fig. 1

Skeletal grains of ilmenite (white) in gangue (dark grey).

(Magnification x 267)

Fig. 2

Exsolution lamellae of magnetite (dark grey - M) within ilmenite (pale grey - Il). The ilmenite has been partially altered to rutile (white - R) and the magnetite to hematite (white - He).

(Magnification x 360)

Fig. 3

Rutile (light grey - R) with 'islands' of ilmenite (dark grey - Il) within it.

(Magnification x 1 200)

Fig. 4

Skeletal grain of goethite (pale grey - Go), formerly magnetite, which is being replaced by bornite (dark grey - Bn) and white chalcocite (white - Cc).

(Magnification x 750)

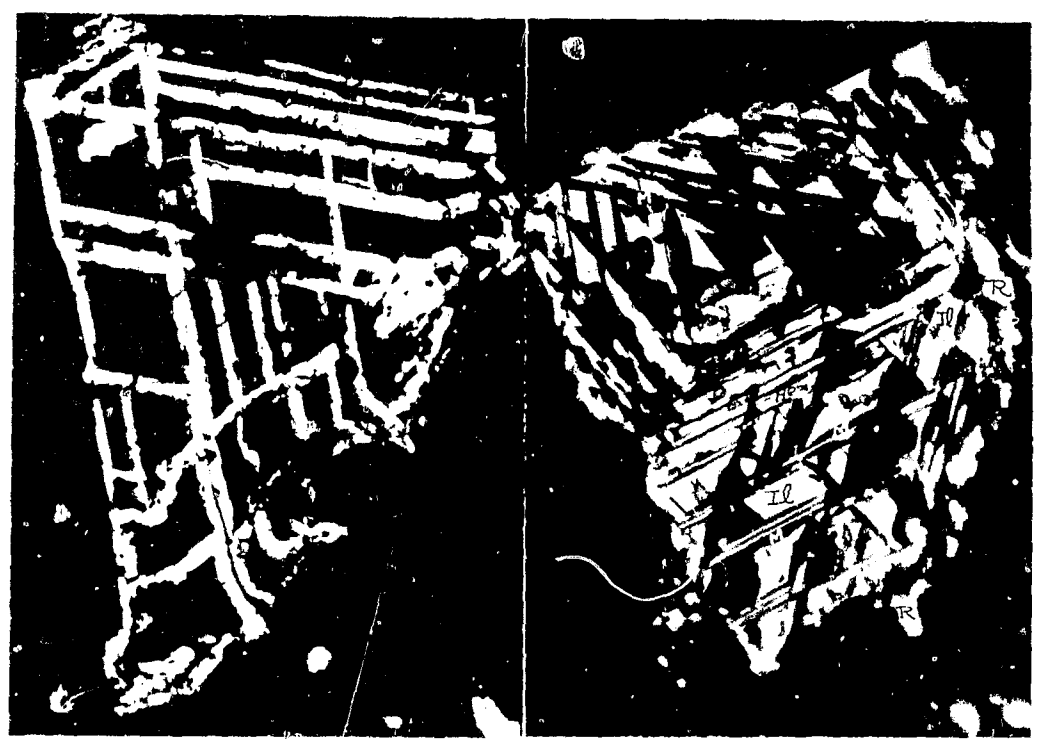
R
Il
R
Il
R

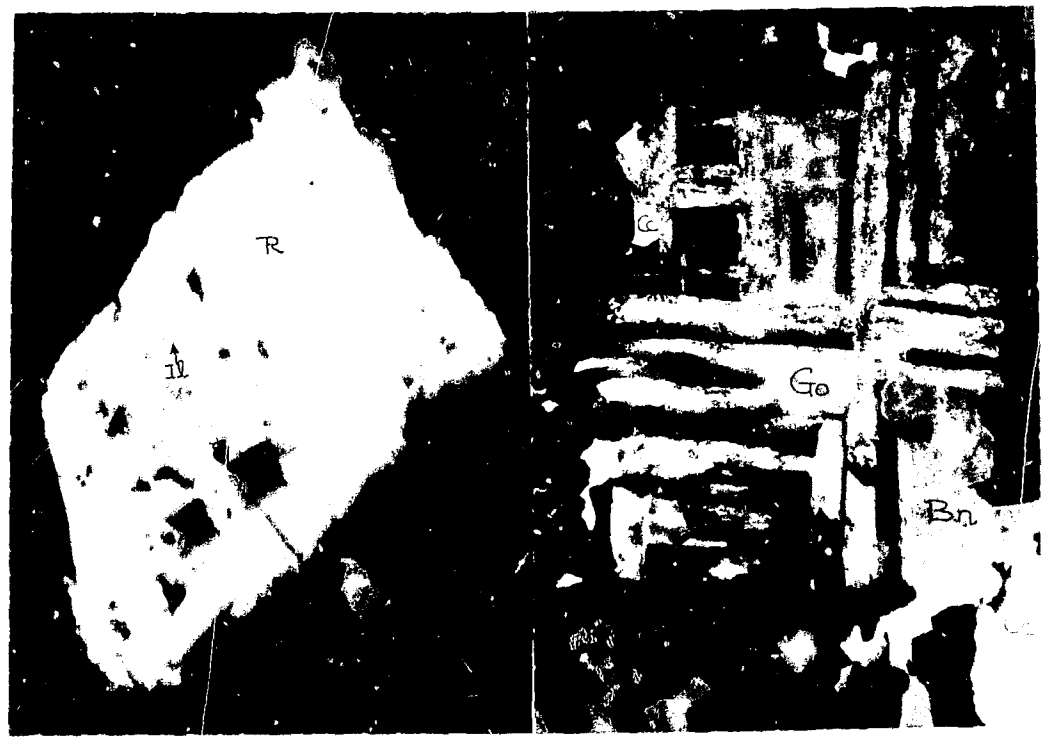
R
Il
G
Go
Bn

Explanation of Plate V

Fig. 1

Photomicrograph of an ilmenite grain (white - Il), which contains exsolution lamellae of magnetite (pale grey - Mg), enclosed completely in goethite (grey - Go) which was formerly magnetite.

(Magnification x 750)

Fig. 2

Photomicrograph showing a composite grain of magnetite and pyrite surrounded by pyrite I (pale grey - Py I) and gangue (black). The composite grain is composed of small 'islands' of magnetite within a 'sea' of pyrite I.

(Magnification x 200)

Fig. 3

Photomicrograph showing chalcopyrite I (white - Cp I) replacing goethite (grey - Go) which was formerly magnetite. The chalcopyrite I is pseudomorphous after magnetite and is replaced by bornite (grey - Bn).

(Magnification x 250)

Fig. 4

Euhedral pyrite I (white - Py I) crystals within amygdaloidal andesite.

(Magnification x 3,4)


CPI
CPI
RI
RI

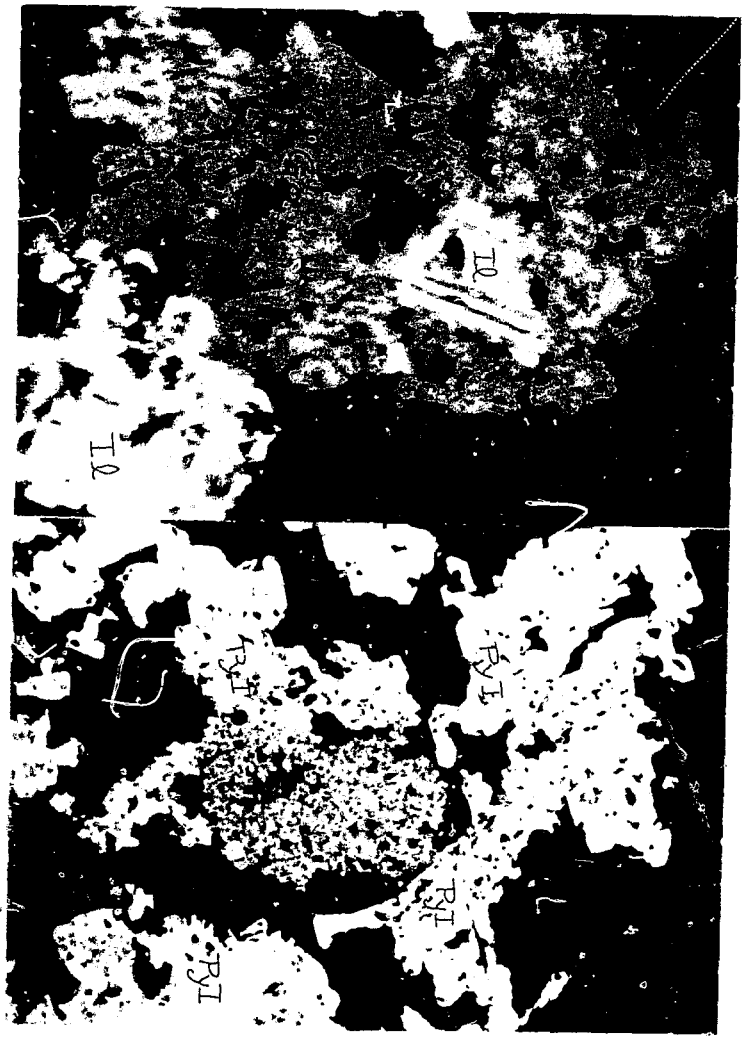
Io
Io
RI
RI
RI
RI

Explanation of Plate VI

Fig.

'Atoll'-like structure formed by pyrite I (white - Py I).

(Magnification x 570)

Fig. 2

Irregular remnants of pyrite I (pale grey with high relief - Py I) present within pyrrhotite (grey - Pyrr). Chalcopyrite I (pale grey with low relief - Cp I) is present as a replacement of the pyrrhotite along its contacts with pyrite I grains.

(Magnification x 800)

Fig. 3

Chalcopyrite I (pale grey with low relief - Cp I) has replaced pyrrhotite (medium grey - Pyrr) in a modified 'caries texture'. The pyrite I inclusions (pale grey with high relief - Py I) within the pyrrhotite, acted as barriers to replacement by chalcopyrite I, and replacement proceeded at a greater rate where the pyrite was absent, so that tongues of chalcopyrite I extended through gaps in the pyrite I barrier and replaced the pyrrhotite beyond.

(Magnification x 750)

Fig. 4

Photomicrograph of pyrite I (pale grey with high relief - Py I) which has been replaced in an 'island and sea' texture by chalcopyrite I (pale grey with low relief - Cp I).

(Magnification x 800)


PyI
PyI
PyI
PyI


PyI
CpI
CpI
PyI
CpI
PyI
CpI
PyI
CpI
PyI

Explanation of Plate VII

Fig. 1

Sphalerite (dark grey - Sph) which has replaced pyrite I (white - Py I) in a 'caries texture' and along cracks. The sphalerite has blobs of chalcopyrite I (white - Cp I) present as exsolution lamellae within it.

(Magnification x 200)

Fig. 2

Photomicrograph of small crystals of pyrite II (white - Py II) lying along irregular lines within sphalerite (dark grey - Sph).

(Magnification x 248)

Fig. 3

Pyrite II (pale grey with high relief - Py II) crystals present in irregular lines cutting across pyrrhotite (grey - Pyrr) and chalcopyrite I (pale grey with low relief - Cp I).

(Magnification x 200)

Fig. 4

Pyrite II (white - Py II) crystals which have formed as a recrystallisation of large earlier formed pyrite I crystals (white - Py I).

(Magnification x 200)

Plate VII

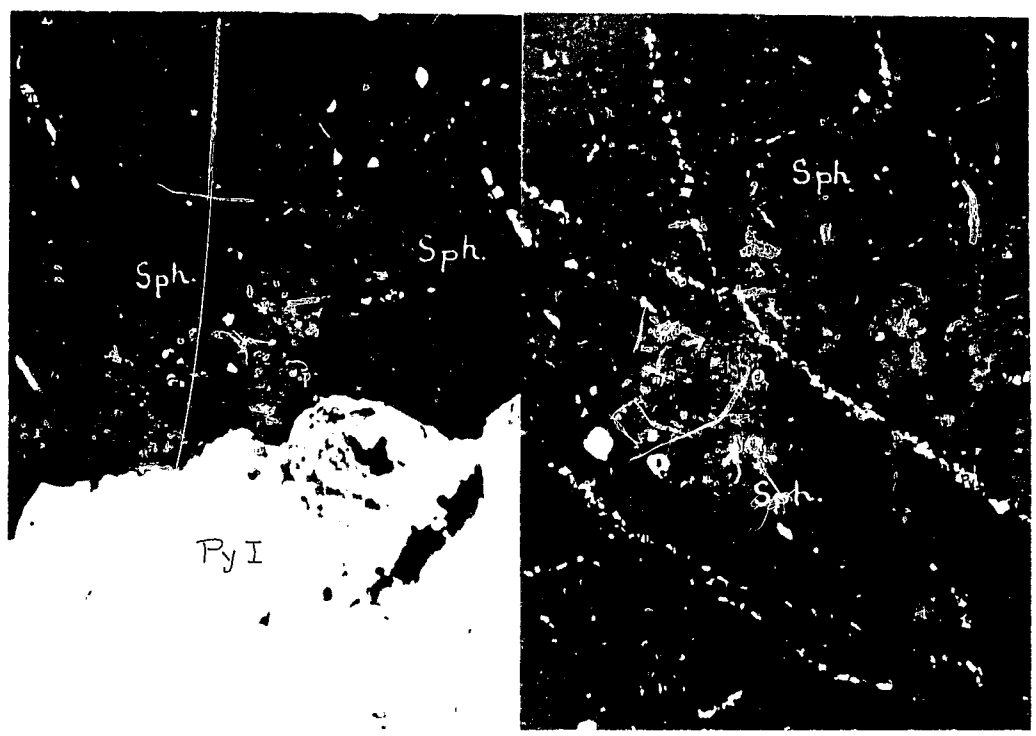

3

4

Explanation of Plate VIII

Fig. 1

Photomicrograph showing a grain of pyrrhotite which has been etched with dilute chromic acid. The hexagonal pyrrhotite (pale grey - Hex.pyrr) is weakly etched and stands out as rounded grains within the strongly etched monoclinic pyrrhotite (dark grey - Mono.pyrr). Grains of pyrite I (white - Py I) have been replaced along their contacts with pyrrhotite by chalcopyrite I (white - Cp I).

(Magnification x 200)

Fig. 2

Exsolution texture of chalcopyrite I (white - Cp I) within sphalerite (grey - Sph).

(Magnification x 800)

Fig. 3

Photograph showing a vein of galena (white - Ga) cutting across sphalerite (pale grey - Sph).

(Magnification x 7,6)

Fig. 4

Photomicrograph showing chalcopyrite I (pale grey - Cp I) which has been partially replaced by pyrrhotite (grey - Pyrr) in a 'caries texture'. However the pyrrhotite itself has been replaced by epidote (black - Ep) which is intruded by chalcopyrite I. Since the pyrrhotite appears to be both older and younger than the chalcopyrite I, this is a mutual texture.

(Magnification x 300)

Plate VIII

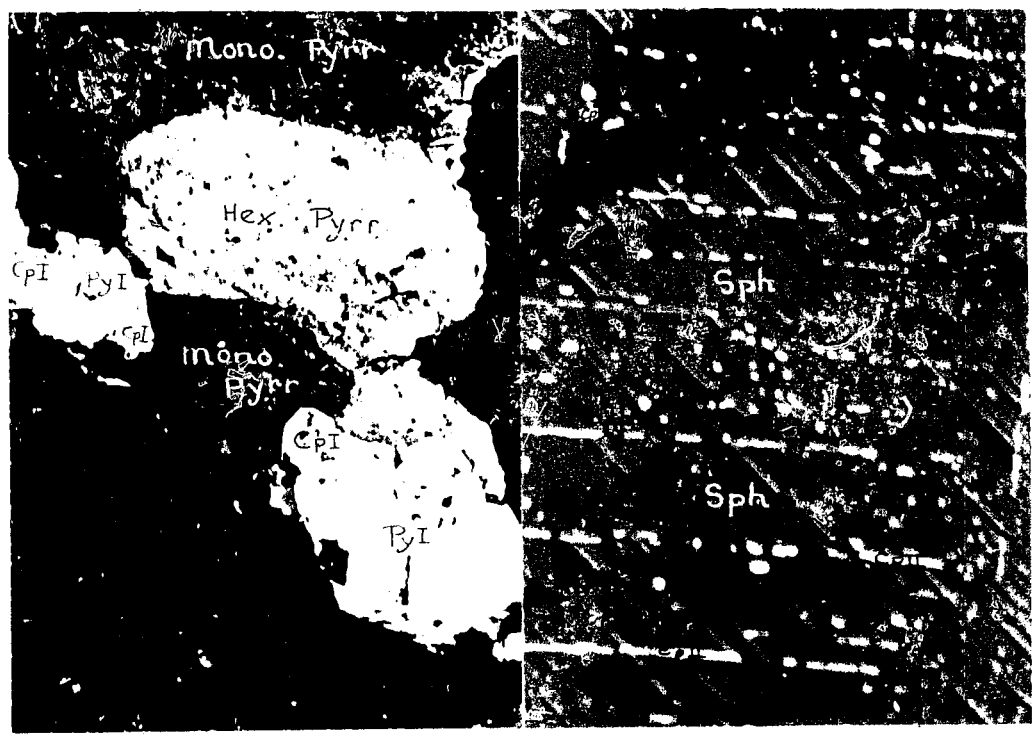
Mono. Pyrr
Hex. Pyrr
CpI
PyI
Mono. Pyrr
CpI
PyI
Sph
Sph

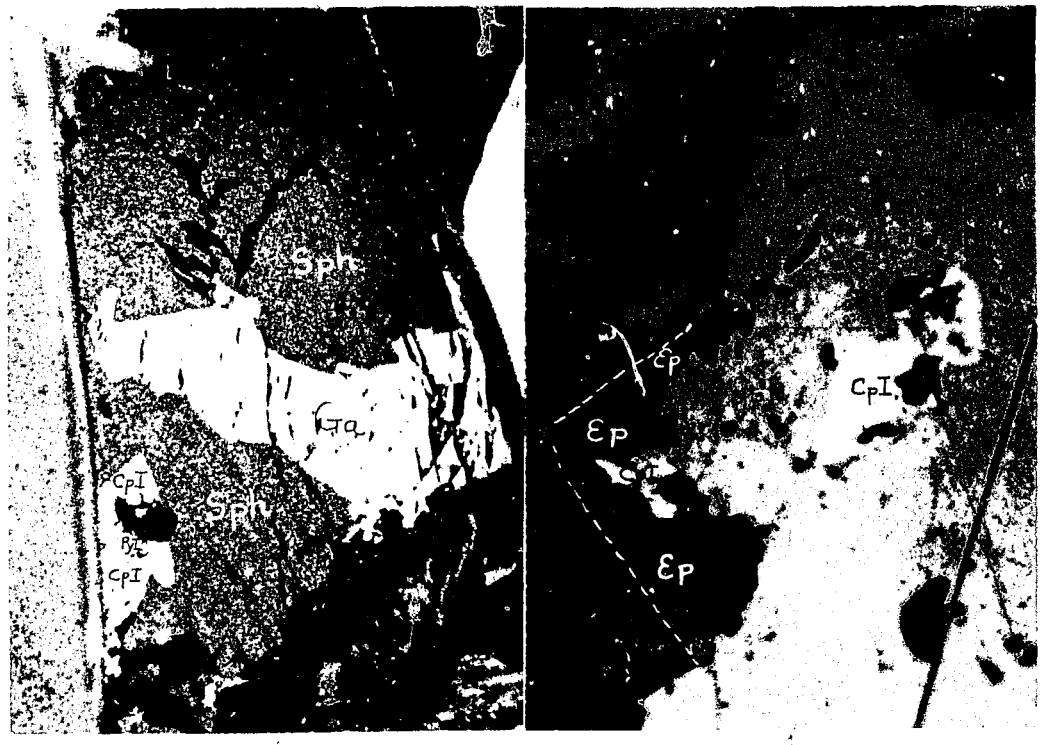
Sph
Fig.
CpI
Sph
CpI
εp
εp
εp
CpI

Explanation of Plate IX

Fig. 1

Remnants of calcite (black) within chalcopyrite I (pale grey - Cp I) which is in turn surrounded and replaced by galena (grey - Ga).

(Magnification x 395)

Fig. 2

Photomicrograph showing exsolution lamellae of chalcopyrite II (white - Cp II) within bornite (pale grey - Bn).

(Magnification x 375)

Fig. 3

Photomicrograph of bornite (grey - Bn) surrounded and replaced by supergene blue chalcocite (pale grey - Cc). Both the bornite and supergene blue chalcocite contain exsolution lamellae of chalcopyrite II (white - Cp II). Covellite (dark grey - Cov) is present as narrow blades replacing the other sulphides. The black material is gangue.

(Magnification x 875)

Fig. 4

Needles of actinolite (black) enclosed within and replaced by chalcopyrite I (white - Cp I). Both minerals being present within an amygdale.

(Magnification x 200)

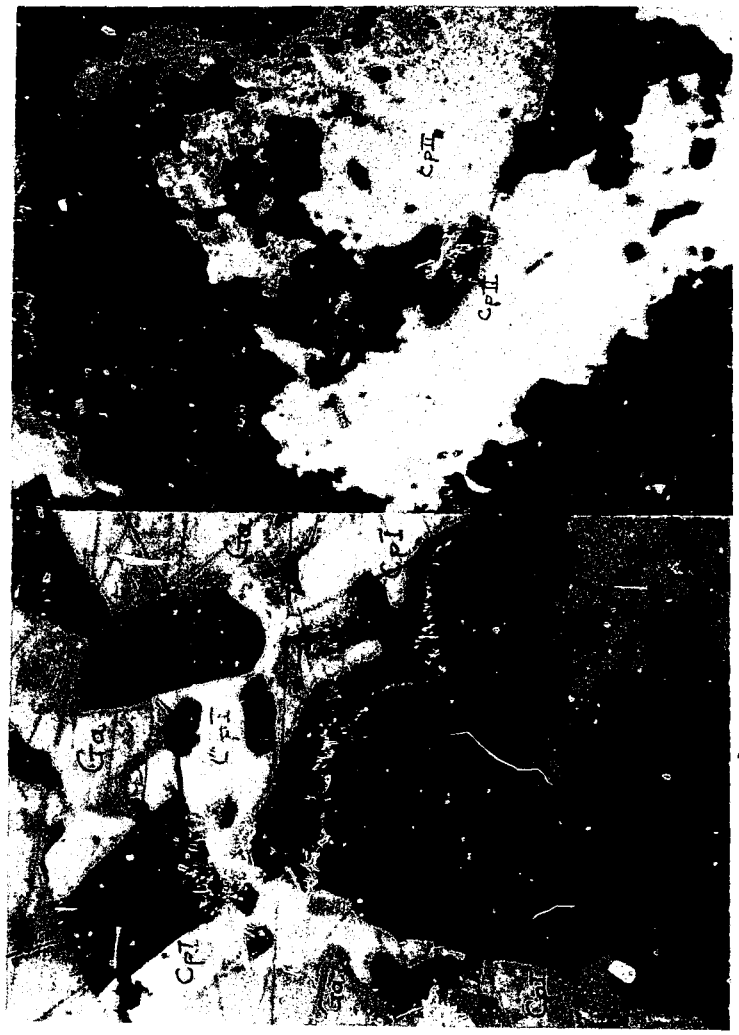

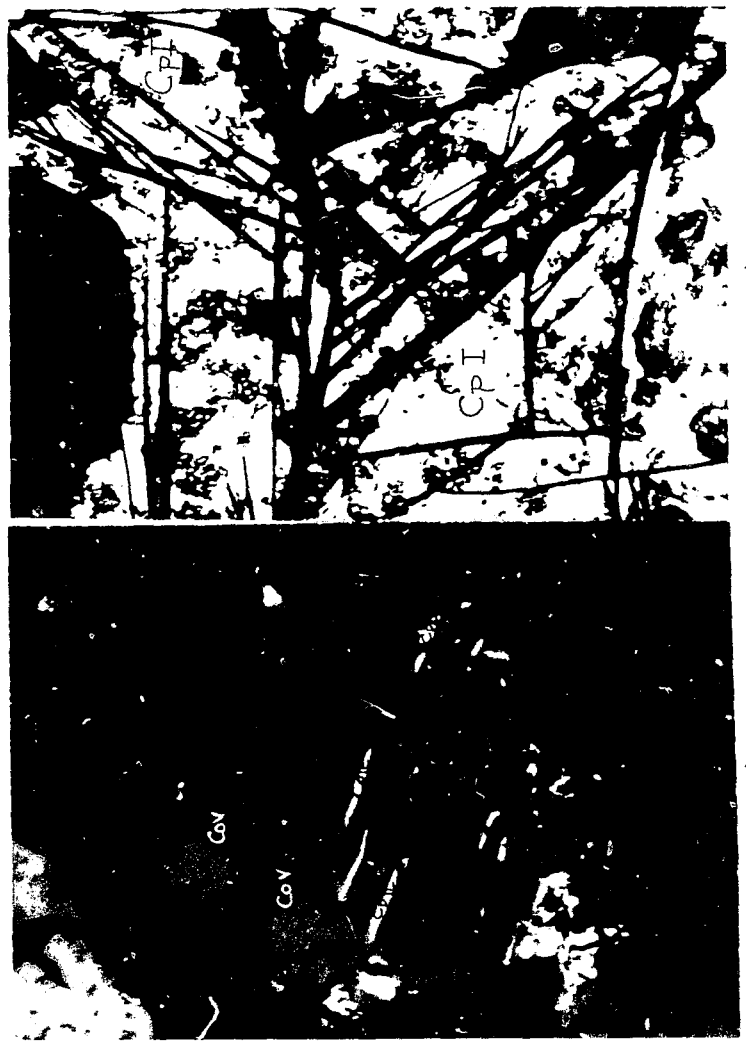

Plate II

Explanation of Plate X

Fig. 1

Epidote (black - Ep) which has been replaced by chalcopyrite I (pale grey - Cp I) in a 'caries texture' and has white chalcocite (grey - Cc) replacing the chalcopyrite I along its contact with the epidote.

(Magnification x 1 000)

Fig. 2

Photomicrograph of 'myrmekitic intergrowth' between white chalcocite (pale grey - Cc) and bornite (dark grey - Bn). A narrow zone of blue chalcocite (grey - bCc) is present between the bornite and the white chalcocite.

(Magnification x 200)

Fig. 3

Vein of white chalcocite (white - Cc) cutting through the gangue (black) and having remnants of bornite (grey - Bn) included within it.

(Magnification x 200)

Fig. 4

Photomicrograph of bornite and white chalcocite which have been etched using a 20 per cent by weight solution of KCN. The white chalcocite (strongly etched - Cc) shows a prominent etch cleavage, it appears to be later formed than the bornite (weakly etched - Bn) since it has 'islands' of bornite within it, and has intruded the bornite along narrow veins.

(Magnification x 800)

Plate X

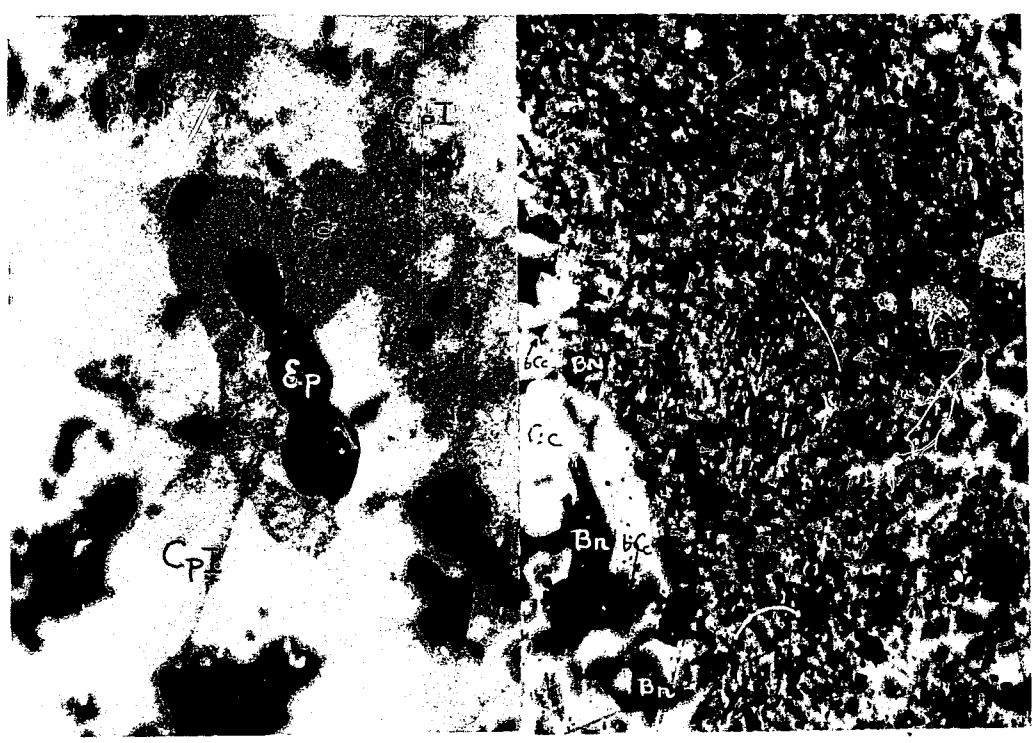

Explanation of Plate XI

Fig. 1

Mutual texture between bornite (dark grey - Bn) and white chalcocite (white - Cc) showing 'islands' of white chalcocite within bornite, which is in turn replaced by white chalcocite. A narrow zone of blue chalcocite (pale grey - bCc) is present between the white chalcocite and the bornite.

(Magnification x 200)

Fig. 2

Photomicrograph showing bornite (dark grey - Bn) with a rim of white chalcocite (white - Cc) along its contact with the gangue (black). There are also two veins of chalcocite cutting through the bornite.

(Magnification x 800)

Fig. 3

Bornite (grey - Bn) is completely rimmed by supergene blue chalcocite (pale grey - Cc).

(Magnification x 750)

Fig. 4

Photomicrograph of an amygdale showing actinolite needles (black) within bornite (grey - Bn) and white chalcocite (white - Cc). The actinolite needles must have been in place before the white chalcocite was formed since they act as divisions between the bornite and white chalcocite.

(Magnification x 267)

Plate XI

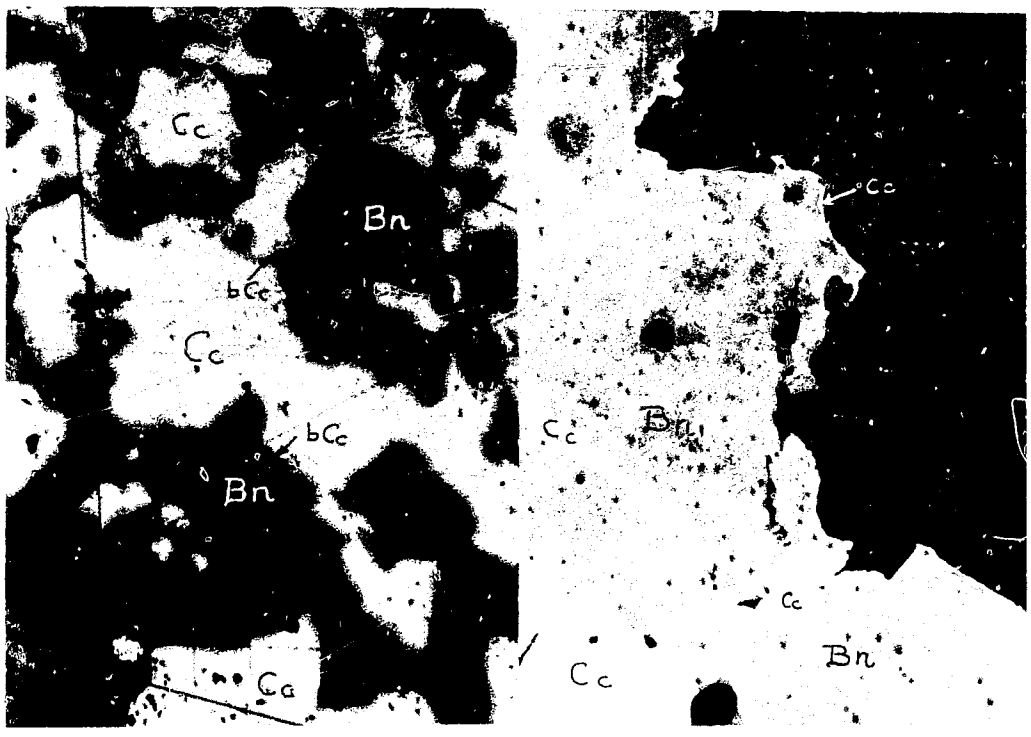

Explanation of Plate XII

Fig. 1

Irregularly shaped grains of covellite (dark grey - Cov) which have replaced white chalcocite (pale grey - Cc).

(Magnification x 750)

Fig. 2

Photomicrograph showing native copper (white - Nat Cu) rimmed by supergene blue chalcocite (grey - Cc). Both copper minerals are surrounded by gangue (black).

(Magnification x 1 690).

Plate XII

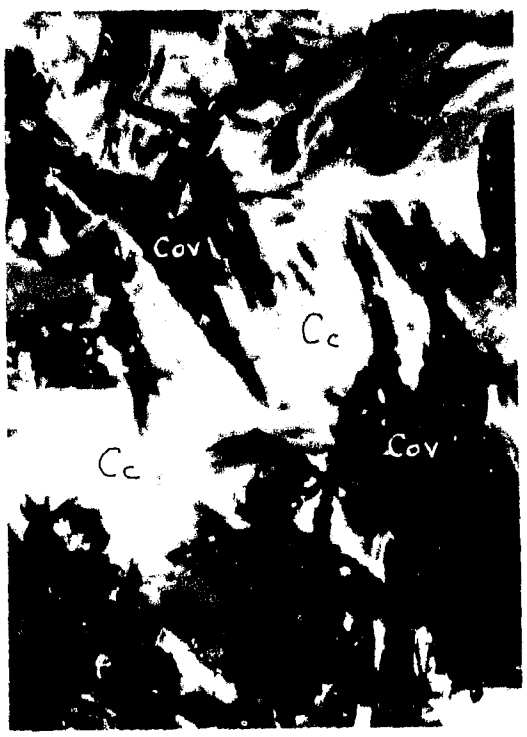

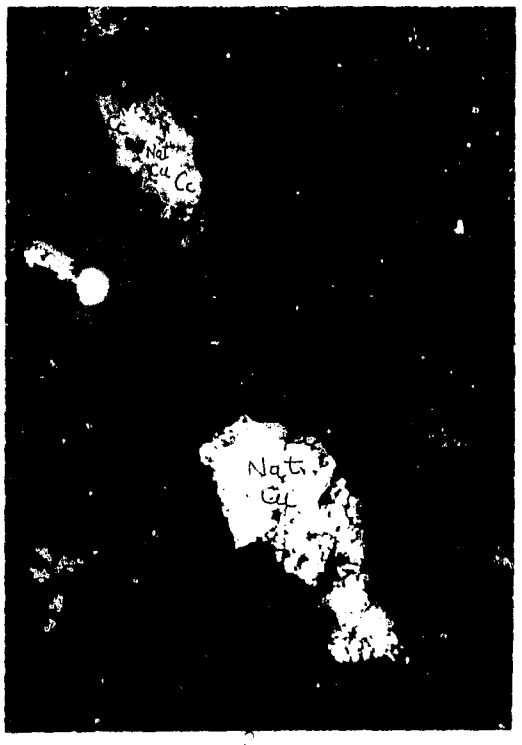

APPENDIX VI

Photomicrographs of Structures and Textures within Thin Sections

Explanation of Plate XIII

Fig. 1

Rounded grains of olivine (pale grey - Ol) within an interstitial groundmass magnetite (black) and biotite (pale grey - Biot).

(Magnification x 200)

Fig. 2

Olivine pseudomorph (dark grey - Bow) with rim of iron oxide (black).

(Magnification x 350)

Fig. 3

Olivine pseudomorph (grey - Bow) partially enclosed within a crystal of pyroxene (pale grey - Px).

(Magnification x 120)

Fig. 4

Phenocrysts of augite (pale grey - Px) partially enclosed within plagioclase phenocrysts (light grey - Pl).

(Magnification x 64)

Plate XIII

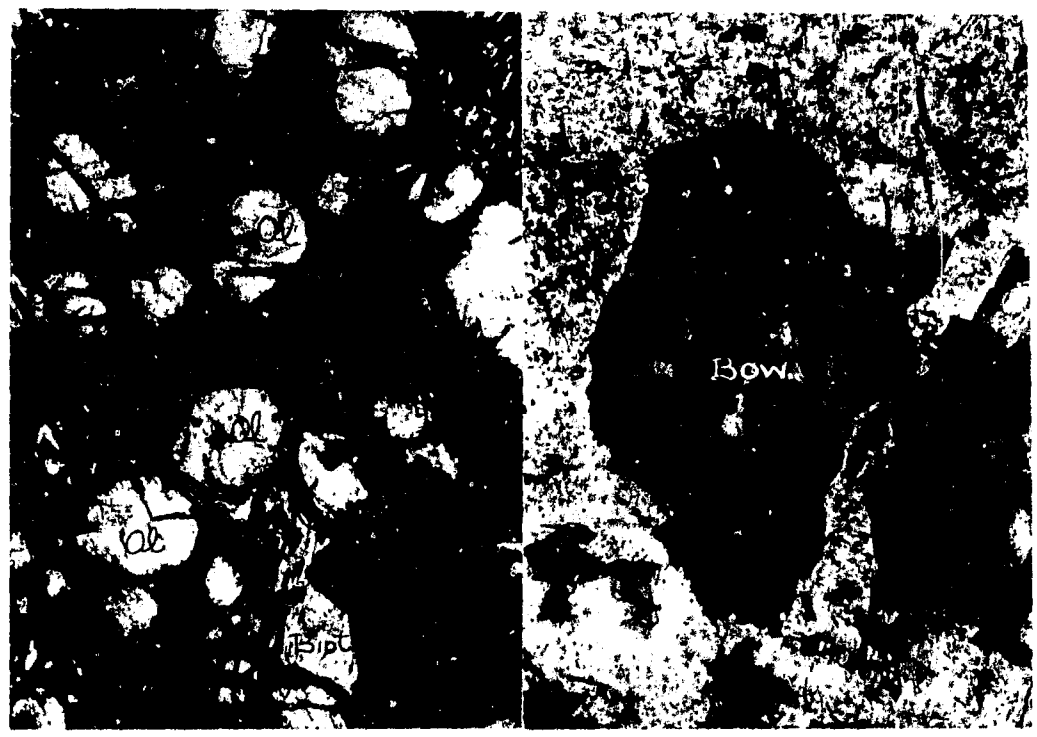

1 2

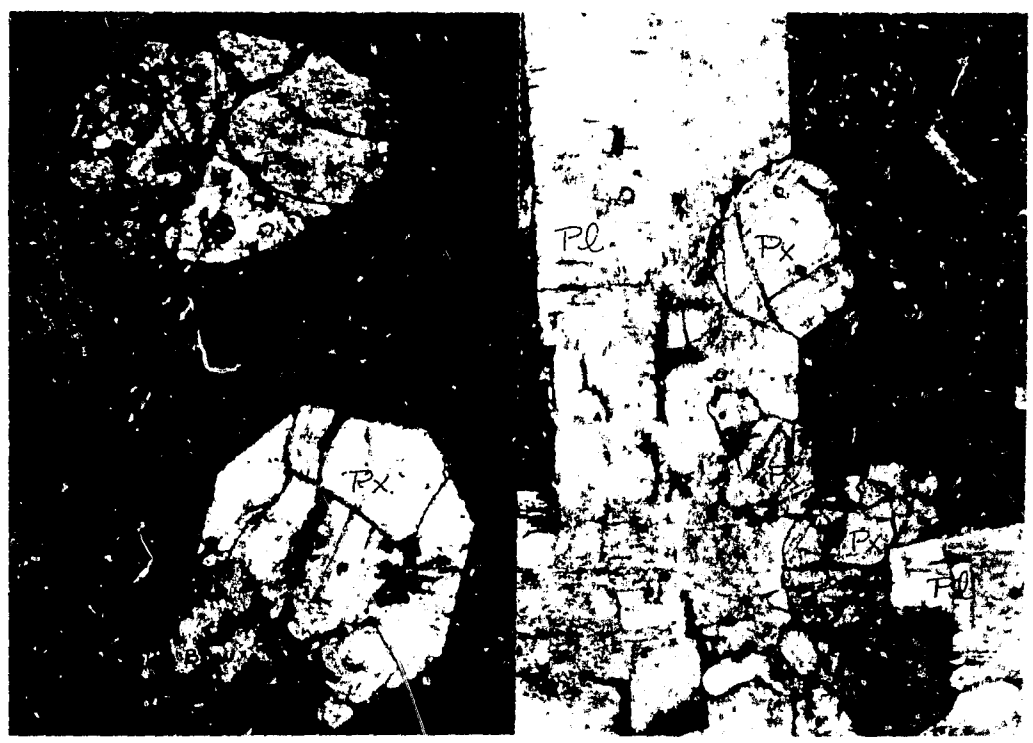

3 4

Explanation of Plate XIV

Fig. 1

Crystal of augite (dark grey and pale grey - Px) showing prominent twinning.

(Magnification x 120)

Fig. 2

Kaersutite (dark grey - K) partially enclosing pyroxene (pale grey - Px).

(Magnification x 240)

Fig. 3

Pyroxene (pale grey - Px) which has been replaced by uralite (grey - Ur) along its edges and cleavages.

(Magnification x 200)

Fig. 4

Kaersutite (dark grey - K) surrounded by biotite (pale grey - Biot).

(Magnification x 240)

Plate XIV

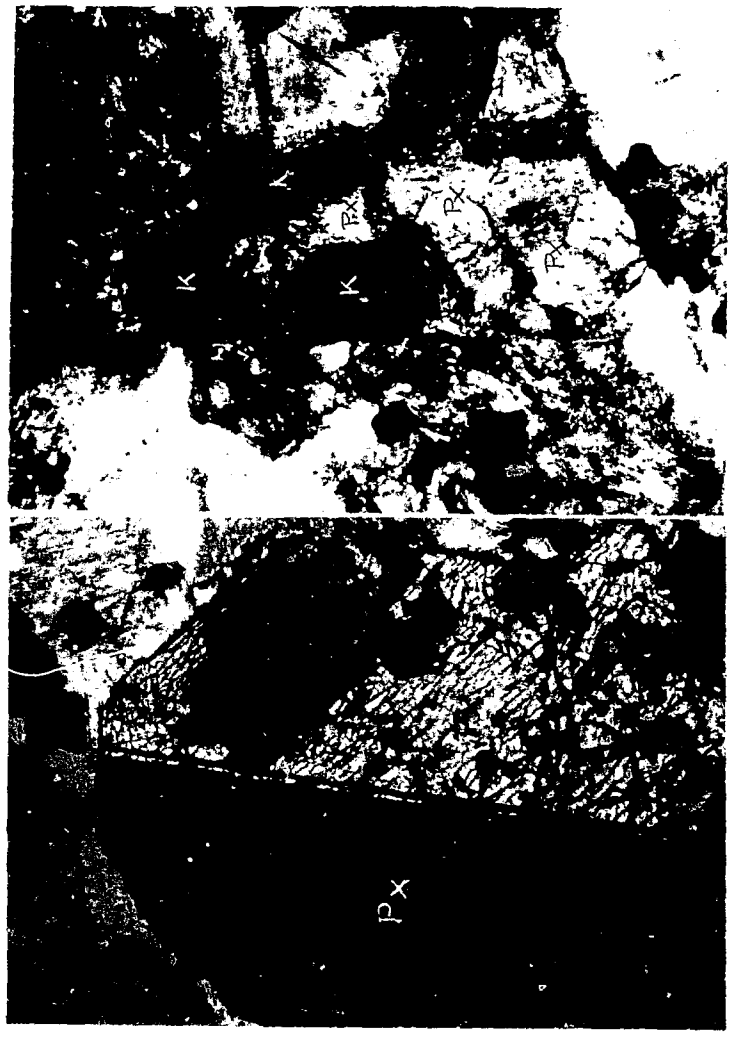

Explanation of Plate XV

Fig. 1

Grain of kaersutite (dark grey - K) with outgrowths of arfvedsonite (grey - Ar) along its edges.

(Magnification x 400)

Fig. 2

Intergrowth of hornblende (dark grey to black - H) and plagioclase (pale grey - Pl).

(Magnification x 28)

Fig. 3

Veins of hornblende (dark grey - H) cutting a crystal of plagioclase (pale grey - Pl).

(Magnification x 240)

Fig. 4

Hematite (black) which is surrounded by plagioclase (pale grey - Pl) within a pegmatite vein.

(Magnification x 120)

Plate XV

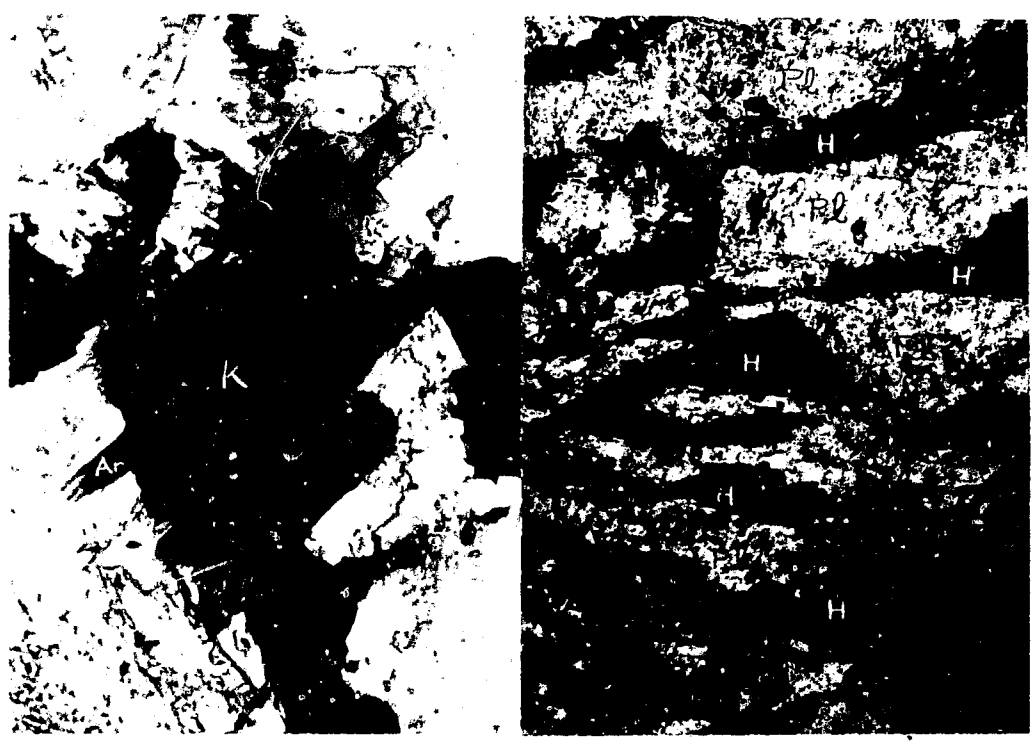

3

4

Explanation of Plate XVI

Fig. 1

Hematite (black) enclosing rock fragments and secondary quartz (white - Q).

(Magnification x 240)

Fig. 2

Amygdale containing calcite (white - Ca) which is surrounded by biotite (black).

(Magnification x 300)

Fig. 3

Calcite (grey - Ca) surrounded by later quartz (pale grey - Q).

(Magnification x 128)

Fig. 4

Amygdale surrounded by quartz (white - Q) and filled with chlorite (mottled grey - Ch) which encloses earlier formed calcite (white - Ca) and biotite (black).

(Magnification x 40)


Ca
Ca
Ca


Ca
Ca
Ca
Ca
Ca
Ca

Explanation of Plate XVII

Fig. 1

Zeolites (white - Z) which have replaced the feldspar within the groundmass of amygdaloidal andesite (light grey - surrounded by stippled line).

(Magnification x 48)